Identification of Iron Carbides in Fe(−Na−S)/α-Al$_2$O$_3$ Fischer-Tropsch Synthesis Catalysts with X-ray Powder Diffractometry and Mössbauer Absorption Spectroscopy

Paalanen, Pasi P.; van Vreeswijk, Sophie H.; Dugulan, A. Iulian; Weckhuysen, Bert M.

Important note
To cite this publication, please use the final published version (if applicable).
Please check the document version above.

ChemCatChem

Full Papers
doi.org/10.1002/cctc.202000707

Chem
Europ

European
Societies P

Check for
updates

Identification of Iron Carbides in Fe(−Na−S)/α-Al$_2$O$_3$ Fischer-Tropsch Synthesis Catalysts with X-ray Powder Diffractometry and Mössbauer Absorption Spectroscopy

Pasi P. Paalanen,[a] Sophie H. van Vreeswijk,[a] A. Iulian Dugulan,[b] and Bert M. Weckhuysen*[a]

In Fe-based Fischer-Tropsch Synthesis (FTS), the Fe carbides form under the carburizing H$_2$:CO reaction atmosphere providing the active phases for hydrocarbon synthesis. H$_2$ reduced Fe (−Na−S)/α-Al$_2$O$_3$ catalyst materials, with and without Na−S promotion, were carburized under CO at 240–440 °C to form Fe carbides. X-ray Powder Diffractometry (XRPD) with Rietveld Quantitative Phase Analysis (R-QPA) and Mössbauer Absorption Spectroscopy (MAS) were used to identity and quantify the formed Fe carbide phases. The Fe carbides formed in order of increasing temperature are ε-Fe$_3$C, η-Fe$_2$C, χ-Fe$_5$C$_2$ and θ-Fe$_3$C. θ-Fe$_7$C$_3$ and a distorted χ-Fe$_5$C$_2$ phase are formed at 25 bar CO (340 °C) from a Fe oxide precursor. Fe carbide formation was unaffected by Na−S addition, but it did increase Fe oxidation (≤ 290 °C) and preferred formation of χ-Fe$_5$C$_2$ over θ-Fe$_3$C phase (≥ 390 °C). The results unify the often ambiguous Fe carbide identification and nomenclature and specify the role of Na−S in the carburization process.

Introduction

In Fe-based Fischer-Tropsch Synthesis (FTS) reaction, Fe phases present under the carburizing H$_2$:CO atmosphere are Fe carbides that form via dissolution of C atoms to zerovalent α-Fe lattice. Under the assumption of the "surface carbide" FTS reaction mechanism, the Fe carbides form the reactive part for the Fe-based FTS reaction dissociating CO and H$_2$.[1] The surface C atoms may then further react to either form hydrocarbons with H atoms or react with other C atoms to form inactive carbon deposits on the catalyst material.[1,2]

In the FTS reaction literature, the Fe carbide phases are commonly identified as (pseudo-)hexagonal or as the "ε-carbides" (ε'-Fe$_{2.2}$C, Fe$_2$C, ε-Fe$_2$C or ε-Fe$_3$C),[3–12] χ-Fe$_5$C$_2$ (the Hägg carbide),[3–5,13–17] θ-Fe$_3$C (cementite),[3–5,18,19] and Fe$_7$C$_3$ (the Eckström-Adcock carbide).[3,5,20–22] While "ε-carbides", χ-Fe$_5$C$_2$ and θ-Fe$_3$C are often observed, the Fe$_7$C$_3$ phase is less common in FTS reaction literature and seems to form under more severe, industrial FTS reaction conditions, than the rest of the carbide phases.[20] From tempering studies on martensitic steel, a Fe carbide labelled as η-Fe$_2$C has been observed.[23] The η-Fe$_2$C phase has been suggested to be closely related to the "ε-carbides" encountered in the FTS reaction research field.[4,11,24]

The most common and suitable characterization techniques applied for identifying the Fe carbide phases present in Fe-based FTS reaction catalyst materials are X-ray Powder Diffractometry (XRPD) and Mössbauer Absorption Spectroscopy (MAS). From the obtained XRPD patterns, the χ-Fe$_5$C$_2$, θ-Fe$_3$C and Fe$_7$C$_3$ phases can readily be identified,[3,5,21,22,25–28] while differentiation between the "ε-carbides" is more challenging with XRPD. In FTS literature, when using XRPD as the characterization method, the precise crystal structures for Fe carbides identified as the "ε-carbides" are often left ambiguous.[3,5,8,12,25,29–33] With MAS, on the basis of the different hyperfine fields, all Fe carbides can be fingerprinted.[4,7,15,16,34–38] Unfortunately, the connection between the experimentally observed Fe carbides and their precise crystal structures from XRPD, in comparison to the assigned hyperfine fields from MAS, is often unclear. This being most evident in the case of the "ε-carbides". Which "ε-carbides" truly exist and with what crystal structures, can be a challenging task to interpret from the literature due to the lack of unified nomenclature between the XRPD and MAS studies.

In our recent review article,[2] we have proposed on the basis of our interpretation of the open literature that the Fe carbides, which form during the FTS reaction are: ε-Fe$_3$C *P6$_3$22* (182), η-Fe$_2$C *Pnnm* (58), χ-Fe$_5$C$_2$ *C2/c* (15), θ-Fe$_3$C *Pnma* (62) and θ-Fe$_7$C$_3$ *Pnma* (62). Of these carbides, we have discussed that the ε-Fe$_3$C and η-Fe$_2$C phases are the Fe carbides cited in the literature as the "ε-carbides" or (pseudo-)hexagonal Fe carbides. For each of the identified Fe carbide phases, we also assigned hyperfine fields for MAS fingerprinting based on the established Fe carbide nomenclature.

The addition of Na−S as chemical promoters on Fe-based FTS reaction catalyst materials increases the CO conversion, α-

[a] P. P. Paalanen, S. H. van Vreeswijk, Prof. Dr. B. M. Weckhuysen
Inorganic Chemistry and Catalysis Group
Debye Institute of Nanomaterial Science
Utrecht University
Universiteitsweg 99
3584 CG Utrecht (The Netherlands)
E-mail: b.m.weckhuysen@uu.nl
[b] Dr. A. I. Dugulan
Fundamental Aspects of Materials and Energy Group
Delft University of Technology
Mekelweg 15
2629 JB Delft (The Netherlands)

value, hydrocarbon products' olefin content and suppresses CH_4 selectivity below expectations from the Anderson-Schulz-Flory (ASF) distribution.[39–42] The addition of the alkali (as Na or K) individually has been observed to stabilize the "ε-carbides",[29,30,43,44] and to decrease the Fe-based catalyst's re-oxidation during the FTS reaction.[43,44]

However, how the combined Na—S promotion affects the formation of the aforementioned Fe carbides is not well known. Also not well known is whether the combined Na—S promotion alters the properties of the individual Fe carbides, providing possible explanations for the observed FTS reaction hydrocarbon selectivity promotion effects.

In this work, we combine ex-situ XRPD with Rietveld Quantitative Phase Analysis (R-QPA) and ex-situ MAS. With these two analytical methods in hand, the Fe carbide formation and properties are studied via CO carburization of supported Fe (—Na—S)/α-Al_2O_3 FTS catalysts with and without Na—S promotion. In more detail, the primary objectives of this study are: i) to experimentally verify the interpretation of the literature,[2] concerning the Fe carbide phases and their formation temperatures; ii) also to establish an experimentally verified, *precise* connection between the MAS hyperfine fields and the Fe carbide crystal structures; and iii) to follow the effect of Na—S promotion on the formation of Fe carbides via CO carburization in terms of phase quantities and possible effects on the crystal lattice parameters. Furthermore, the effect of Na—S promotion on morphological changes and carbon deposition on the CO carburized Fe(—Na—S)/α-Al_2O_3 catalyst materials were studied. Both, Transmission Electron Microscopy (TEM) and Thermogravimetric Analysis with combined Mass Spectrometry (TGA-MS) are employed for this purpose. These results are given in Supporting Information.

Results and Discussion

In order to facilitate the comparison of the XRPD-derived R-QPA results and MAS quantifications for the various catalyst materials, a shorthand notation is used, as outlined in Table 1. The shorthand notation of *240, 290, 340, 390* or *440* refers to the applied CO carburization temperature of the H_2 reduced catalyst at atmospheric pressure. Catalyst materials CO carburized *directly* after the calcination step at 25 bar CO pressure at 340 °C are noted in shorthand as *340 h.p.* Notation *Calcin.* is used for catalyst materials characterized directly after applying the calcination step. Likewise, notation *H_2* is used for the H_2 reduced catalysts. The shorthand notation *UP* is used for

unpromoted Fe/α-Al_2O_3, while *Na-S* is used for the Na—S promoted Fe—Na—S/α-Al_2O_3 catalyst on which the catalyst treatments have been applied to. Throughout the results and discussion within this study, the Fe carbide identification and nomenclature given in our recent review article is followed.[2] This nomenclature has also been applied to interpret the identity for the Fe carbide phases from the cited and discussed references within this work.

Phase Quantification with X-ray Powder Diffractometry/Rietveld Quantitative Phase Analysis and Mössbauer Absorption Spectroscopy

Figure 1 shows the background-corrected, ex-situ XRPD measured and the Rietveld method calculated diffraction patterns with their difference to the experimentally measured XRPD patterns, for the Calcin. and H_2 catalysts. The X-ray diffraction patterns after CO carburization are given in Figure 2 for the UP and in Figure 3 for the Na—S catalyst materials. For sake of clarity, only the range 13–29° 2θ Mo K_α, where the Fe carbides show their most intense diffraction peaks, is shown in these figures. R-weighted pattern (R_{wp}) values for the Rietveld fits are given in Figure S1.[45] The MAS spectra with fitted phase peaks for the UP catalysts after H_2 and carburizing 240–440 and 340 h.p. treatments are given in Figure 4. The MAS spectra for the Na—S catalysts are omitted, as the spectra were very similar to those of the corresponding UP catalysts.

The crystalline Fe phase quantifications with R-QPA and the corresponding quantification results as based on the MAS measurements are presented in Figure 5. The used MAS fit details are given in Table S1 for the UP and in Table S2 for the Na—S catalyst materials. The R-QPA and MAS quantifications are in good agreement with each other. The R-QPA quantification results for the Fe phases in the Calcin. catalyst, which only quantified as α-Fe_2O_3 (hematite) for both UP and Na—S catalysts, are excluded from Figure 5b. These quantification results were nevertheless used for calculating the elemental Fe contributions for the UP and Na—S Calcin. catalyst materials in Figure 5c.

The R-QPA derived elemental Fe contributions do not change significantly between the studied catalysts. The mean elemental Fe wt-%s are for UP catalyst materials 6.4 ± 0.5 wt-% and for Na—S materials 6.7 ± 0.5 wt-%, in comparison between all of the applied treatments within their promotion groups (Figure 5c). This matches well with the ICP-OES quantification results that indicated the presence of ≈ 6.6 wt-% of elemental Fe for both the parent UP and Na—S Calcin. catalyst materials

Table 1. Overview of the catalyst treatments and the used shorthand notation in this study. The treatments were performed on supported Fe(—Na—S)/α-Al_2O_3 catalyst materials with or without the Na—S promotion.

Shorthand Notation	Catalyst Material Description
Calcin.	Calcining in air at 500 °C for 6 h
H_2	H_2 reduction at 400 °C for 5 h, after the calcining step
240, 290, 340, 390, 440	CO carburization (at 1 atm) temperature in °C, after the reduction step
340 h.p.	CO carburization at 25 bar at 340 °C, after the calcining step
UP	Unpromoted Fe/α-Al_2O_3 catalyst
Na—S	Na—S promoted Fe—Na—S/α-Al_2O_3 catalyst

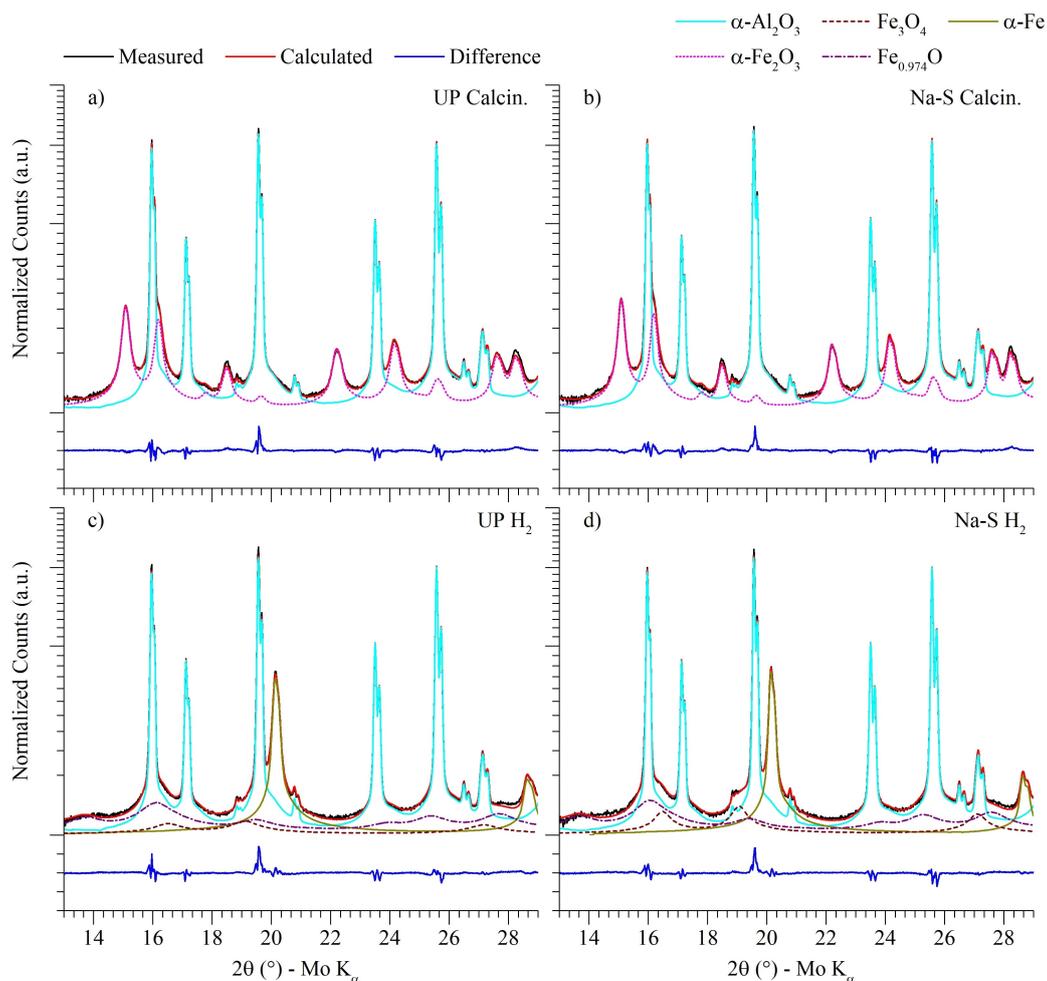**These are not the final page numbers!** ↗↗

Figure 1. Background corrected, ex-situ measured X-ray Powder Diffractometry (XRPD) and Rietveld method calculated diffraction patterns over a range 13–29° 2θ for UP a) Calcin. and c) H$_2$; and for Na–S b) Calcin. and d) H$_2$ treated catalyst materials (Fe(–Na–S)/α-Al$_2$O$_3$). Normalized counts are on a square-root scale.

(Table 4). The good match between the ICP-OES (parent materials) and R-QPA derived elemental Fe values can be taken as an indication that all of the Fe phases present in the catalyst materials have been fitted consistently with a correct calculated Fe crystal structure.

As a general note on performing bulk characterization studies on zerovalent Fe-based materials: a $\approx$ 4–5 nm Fe re-oxidation shell layer is expected to form upon exposure of the catalyst to air or another source of O atoms.[46,47] Such layer on Fe is indeed observable in TEM figures, as can be noted in e.g. Figure S3b. This effectively decreases the crystalline content of the Fe carbides from what they were during the application of each catalyst treatment. This leads to a general recommendation: at least a $\approx$ 20 nm Fe particle diameter is needed in order to preserve sufficient quantities of Fe carbides for a bulk characterization technique study, as is done in this work (Figure S5). However, Fe particles smaller than $\approx$ 10 nm by diameter would be increasingly or solely measured as Fe oxides in bulk quantification studies due to the re-oxidation by O atoms, skewing the quantification results.[16,48]

Effect of H$_2$ Reduction

After applying a H$_2$ reduction treatment, both the UP and Na–S catalysts are well reduced into α-Fe. This observation is valid regardless of the reduction retarding effect of alkali in the Na–S catalysts,[49] and possible catalyst material re-oxidation upon exposure of zerovalent Fe to air.[46,47,50]

All catalysts under study were cooled down under N$_2$ or N$_2$:H$_2$ flow and flushed with N$_2$ at room temperature for a period of time, without a dedicated passivation step.[47] No detrimental re-oxidation of α-Fe is observed in the H$_2$-treated catalysts, which implies that the oxygen-containing impurities in the input N$_2$ gas sufficiently passivate the catalysts for the present bulk Fe study purposes. $\approx$ 4 nm passivation layer is formed (e.g. Figure S3b), which corresponds to what has been also achieved with a dedicated O$_2$ passivation step.[47]

Furthermore, the Fe oxide content quantifications of 31% of Fe$_3$O$_4$ (magnetite) with R-QPA and 15–17% of Fe^{3+} (Super-paramagnetic, SPM) with MAS are in discrepancy with each other (Figure 5a). This Fe oxide content is likely due to the

These are not the final page numbers! ⬀⬀

ChemCatChem

Full Papers
doi.org/10.1002/cctc.202000707

Chemistry Europe
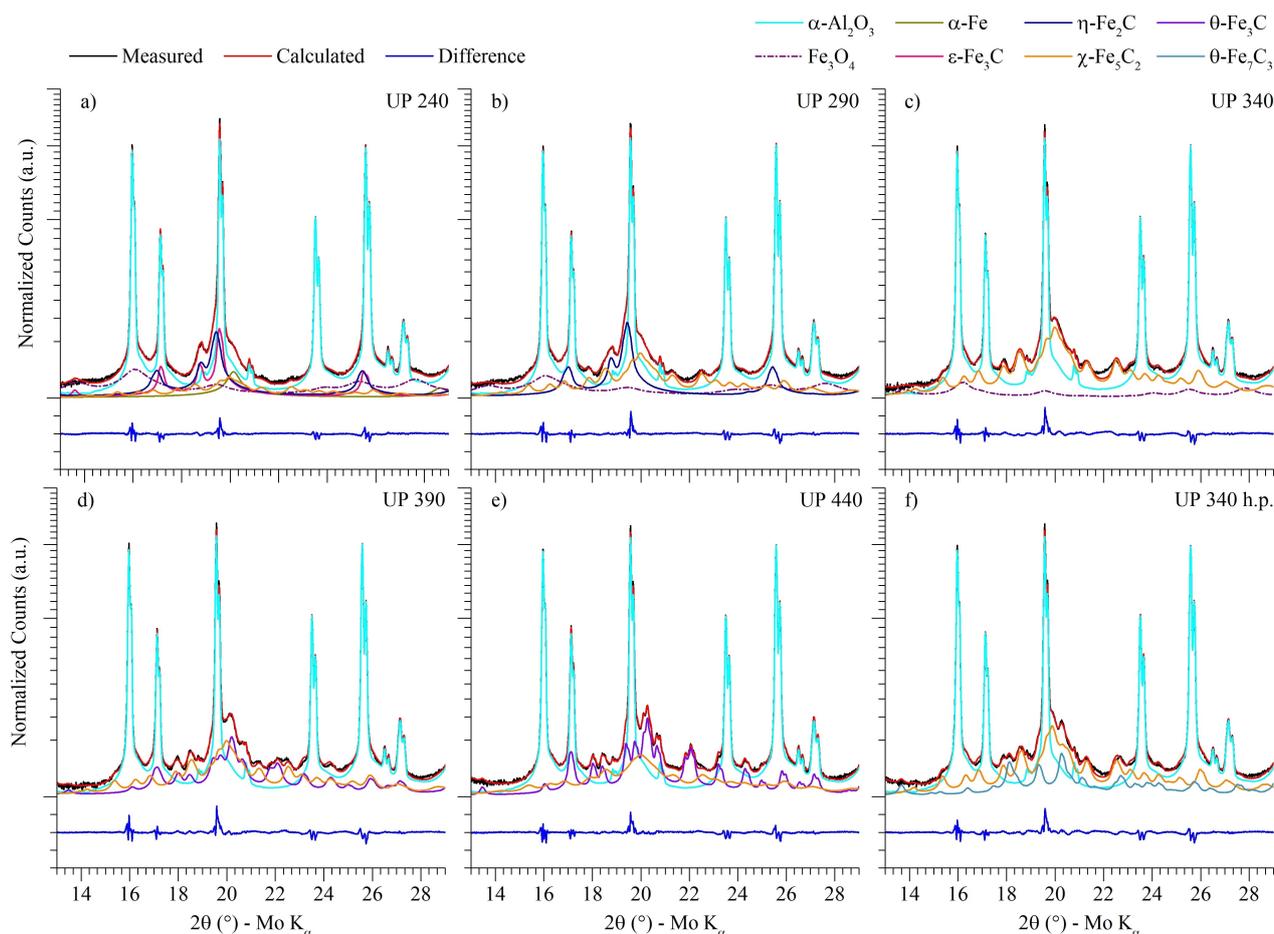European Chemical
Societies Publishing

Figure 2. Background corrected, ex-situ measured X-ray Powder Diffractometry (XRPD) and Rietveld method calculated diffraction patterns over a range 13–29° 2θ for the UP (Fe/α-Al$_2$O$_3$) catalyst materials after the respective catalyst treatment. The diffraction patterns as after catalyst treatment a) 240, b) 290, c) 340, d) 390, e) 440 and f) 340 h.p.. Normalized counts are on a square-root scale.

formed passivation layer,[46,47] which is hard to quantify with the bulk characterization techniques applied in this study. Room temperature MAS underestimates the quantity of Fe oxides in the thin passivation layer.[50] This explains the decreased Fe oxide content with MAS quantifications for H$_2$-treated catalysts.

MAS measurements at 4.2 K would improve the quantification accuracy of the Fe oxide/hydroxide surface layer with respect to the room temperature MAS used in this work.[50,51] The XRPD-based data is naturally less accurate with poorly crystalline,[52,53] and/or with small ≲ 4–5 nm crystallite diameter phases. The R-QPA fitted Fe$_3$O$_4$ phase (shown in Figure 1c–d) gives very weak and broad X-ray diffraction peaks with very small estimated crystallite diameters of ≈3 nm (Figure S8). Thus, some inaccuracy can be expected in this study in the determined Fe oxide phases' quantities due to the used characterization techniques. Furthermore, although the Fe$_3$O$_4$ crystal structure is used in the R-QPA fits, using ferrihydrite structures instead of Fe$_3$O$_4$ also resulted in similar overall R-QPA fits (the fits are not shown for brevity).[54]

In the Na–S H$_2$ catalysts, the presence of 12% of Fe$_{0.974}$O (wüstite) phase is enhanced in the R-QPA phase quantification

as a difference to the UP H$_2$ catalysts with only 5% of the Fe$_{0.974}$O phase present (Figure 5b). Various chemical interactions between the Fe and support materials or other added compounds, such as alkali K, can stabilize the wüstite phase.[55] Thus, the Na–S promotion somewhat stabilizes the Fe$_{0.974}$O phase. The α-Al$_2$O$_3$ support does not play a role in the stabilization as the UP H$_2$ catalyst does not have a significant Fe$_{0.974}$O phase content. No clear presence of the Fe$_{0.974}$O phase was detected with any of the MAS quantifications (Figure 5a).

Effect of Carburization Temperature

Increasing the CO carburization temperature shifts the Fe carbide phase formation from the α-Fe starting material in the following order: ε-Fe$_3$C < η-Fe$_2$C < χ-Fe$_5$C$_2$ < θ-Fe$_3$C. This can be observed in the Fe phase quantification data (Figure 5a–b). This order is also in agreement with the Fe carbide temperature evolution interpreted from the literature, when following the identification and nomenclature proposed for the Fe carbides in our recent review article.[2] With a short CO carburization time
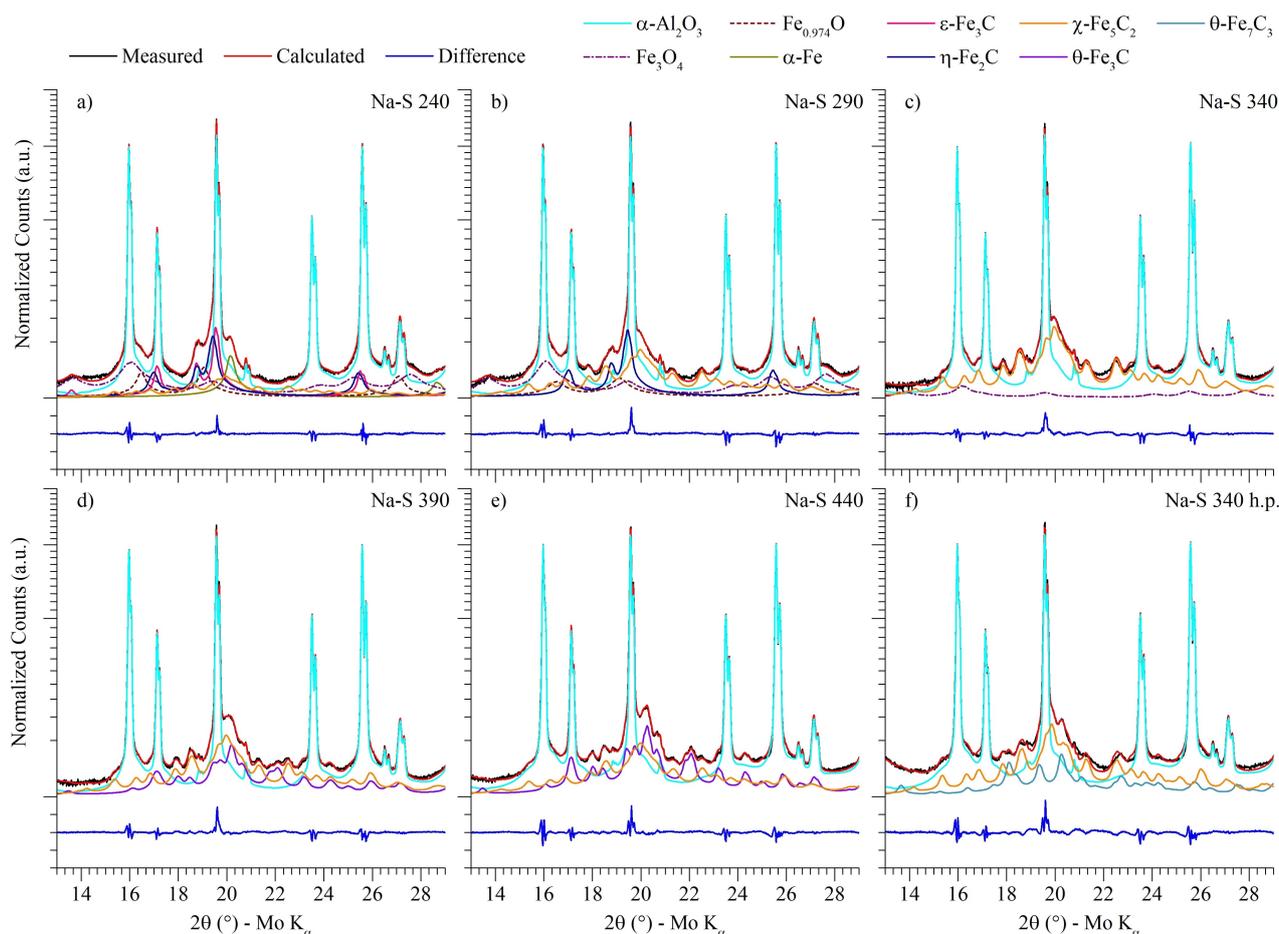
ChemCatChem

Full Papers
doi.org/10.1002/cctc.202000707

Chemistry Europe
European Chemical
Societies Publishing

Figure 3. Background corrected, ex-situ measured X-ray Powder Diffractometry (XRPD) and Rietveld method calculated diffraction patterns over a range 13–29° 2θ for the Na–S (Fe–Na–S/α-Al₂O₃) catalyst materials after the respective catalyst treatment. The diffraction patterns as after catalyst treatment a) 240, b) 290, c) 340, d) 390, e) 440 and f) 340 h.p.. Normalized counts are on a square-root scale.

of ≤3 h at temperatures ≤290°C, also Fe oxide phases are present in the catalysts, in addition to the Fe carbides. The shorter carburization times for ≤290°C treatments were used in order to maximize formation of ε-Fe₃C over η-Fe₂C at 240°C,[34] and to minimize formation of χ-Fe₅C₂ at 290°C.[8,19]

The formation of θ-Fe₇C₃ phase with the catalyst treatment 340 h.p. is discussed separately after the other CO carburization treatments and Fe carbides. Its formation is a more complex, and not a solely temperature-dependent phenomenon.

Effect on Fe Oxides

When moving from the catalyst treatment H₂ to the treatments 240 and 290, the Fe oxide (Fe₃O₄/Fe³⁺ SMP) content in the catalysts increase, according to the quantification results (Figure 5a). When comparing the XRPD patterns for the catalyst treatments H₂ UP and Na–S (Figure 1c–d), 240 and 290 UP (Figure 2a–b) and 240 and 290 Na–S (Figure 3a–b), the X-ray diffraction originating from the fitted Fe₃O₄ phase (e.g. at 27.62° 2θ) is increased after applying the catalyst treatments

240 and 290. The total MAS (Fe³⁺) and R-QPA (Fe₃O₄+Fe₀.₉₇₄O) quantifications of the Fe oxide phases are in fair agreement for the catalyst treatments 240 and 290. Thus, an increased crystallinity of the Fe oxide phases (Fe₃O₄+Fe₀.₉₇₄O) in respect to the H₂ treated catalyst materials improves the accuracy of the quantification results in the cases of 240 and 290 treated catalysts.

The increased Fe oxide crystallinity/content could possibly be due to the O from CO dissociation during the CO carburization behaving as an oxidation agent.[56] As possible explanations we can put forward: i) O from dissociated CO is poorly removed as CO₂,[57,58] with the short applied CO treatment time of <3 h and/or due to the low reaction temperature of <290°C; and/or ii) the O-removal product CO₂ causes the oxidation of α-Fe downstream in the catalyst bed.[20,31,59–61]

Any re-oxidized Fe is expected to reduce poorly back to α-Fe for (re-)carburization by CO, with the applied reduction temperatures ≤290°C.[55] Low amounts of (≈1%) H₂ in the CO stream increase the CO dissociation rate over α-Fe.[62,63] H₂ possibly removes surface O from dissociated CO as H₂O more efficiently than CO does as CO₂. When a low temperature (≲

ChemCatChem

Full Papers
doi.org/10.1002/cctc.202000707
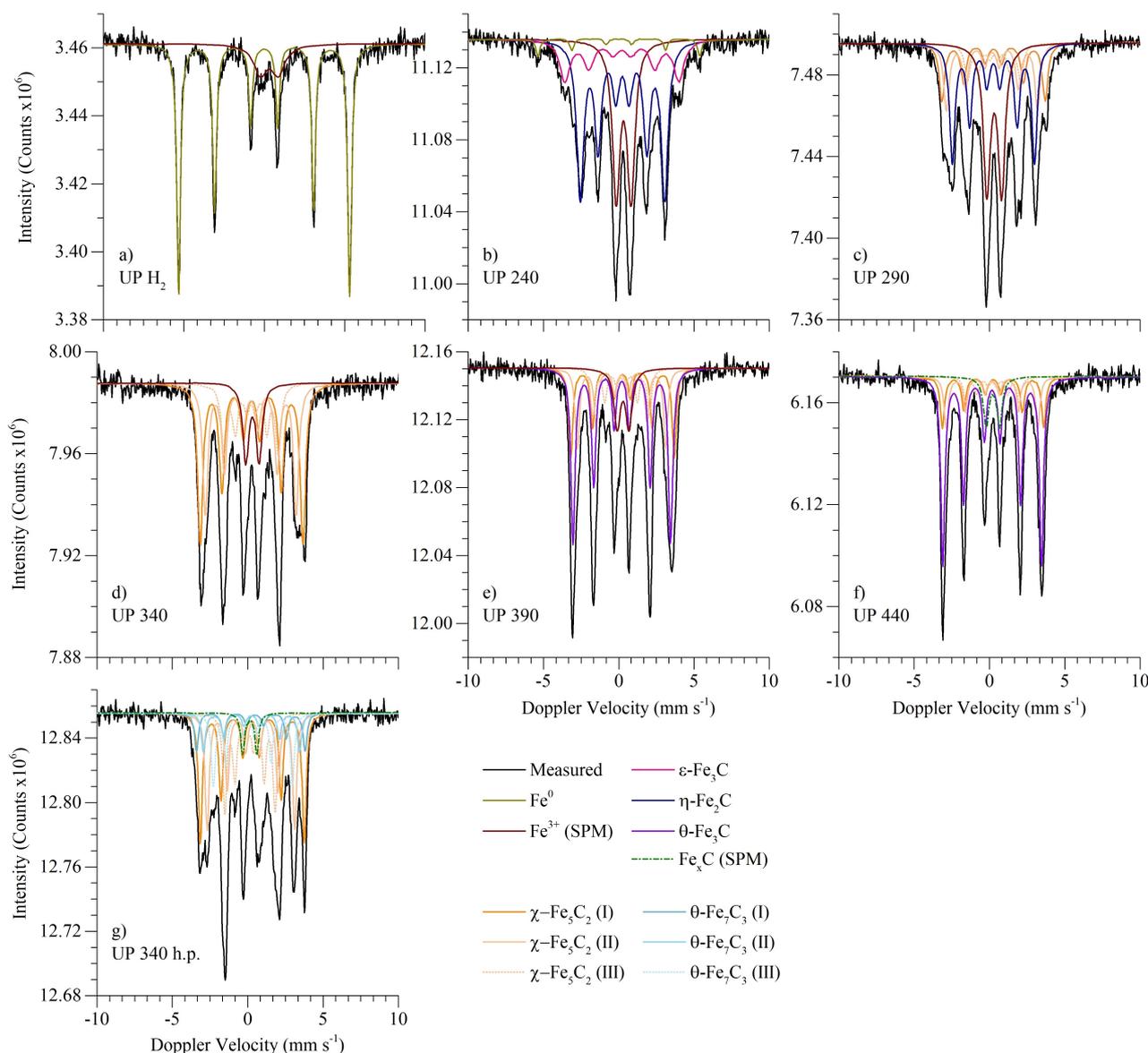
Chemistry Europe
European Chemical
Societies Publishing

Figure 4. Ex-situ measured Mössbauer Absorption Spectroscopy (MAS) spectra with fitted patterns for the Fe phases for the UP (Fe/α-Al$_2$O$_3$) catalyst materials. The MAS spectra as measured at room temperature (300 K) after catalyst treatment a) H$_2$, b) 240, c) 290, d) 340, e) 390, f) 440 and g) 340 h.p.. The Roman numbers (I, II, III) mark the different non-equal Fe positions fitted for the Fe phases. SPM = superparamagnetic.

235 °C) carburization step is performed with a H$_2$:CO mixture, instead of pure CO, the resulting Fe oxidization degree in the Fe carburization process might be decreased.[15] Or alternatively, O-free hydrocarbons can also be used for the α-Fe carburization to decrease the re-oxidation of Fe.[56]

Thus, indirectly, the quantification results for the 240 and 290 catalysts can be interpreted to support the thought of the Fe oxidation via poor removal of O from CO dissociation by CO only. In addition, the oxidative effect by CO$_2$ can participate into the Fe re-oxidation process, but this effect is harder to determine based on our results. Also worth noting is that the addition of Na–S promoters increases the Fe oxide formation after the catalyst treatments 240 and 290, from 18–27 % for UP

up to 41 % for Na–S catalyst materials (Figure 5a). This oxidation effect will be discussed more later on with rest of the Na–S promotion effects on Fe carburization.

The Fe oxide content decreases with respect to the H$_2$ catalyst materials with the catalyst treatments with longer CO exposure times of $\geq$ 16 h and above temperature of 340 °C, i.e. with the treatments 340, 390, 440. This is observed with both the R-QPA and MAS quantifications (Figure 5a–b). That is, possible catalyst materials' oxidation by O from the CO dissociation does not play a role, and the catalyst materials' re-oxidation by air exposure is also decreased. Both the higher carburization temperature and the increased CO exposure time are expected to improve the O removal as CO$_2$, and to increase
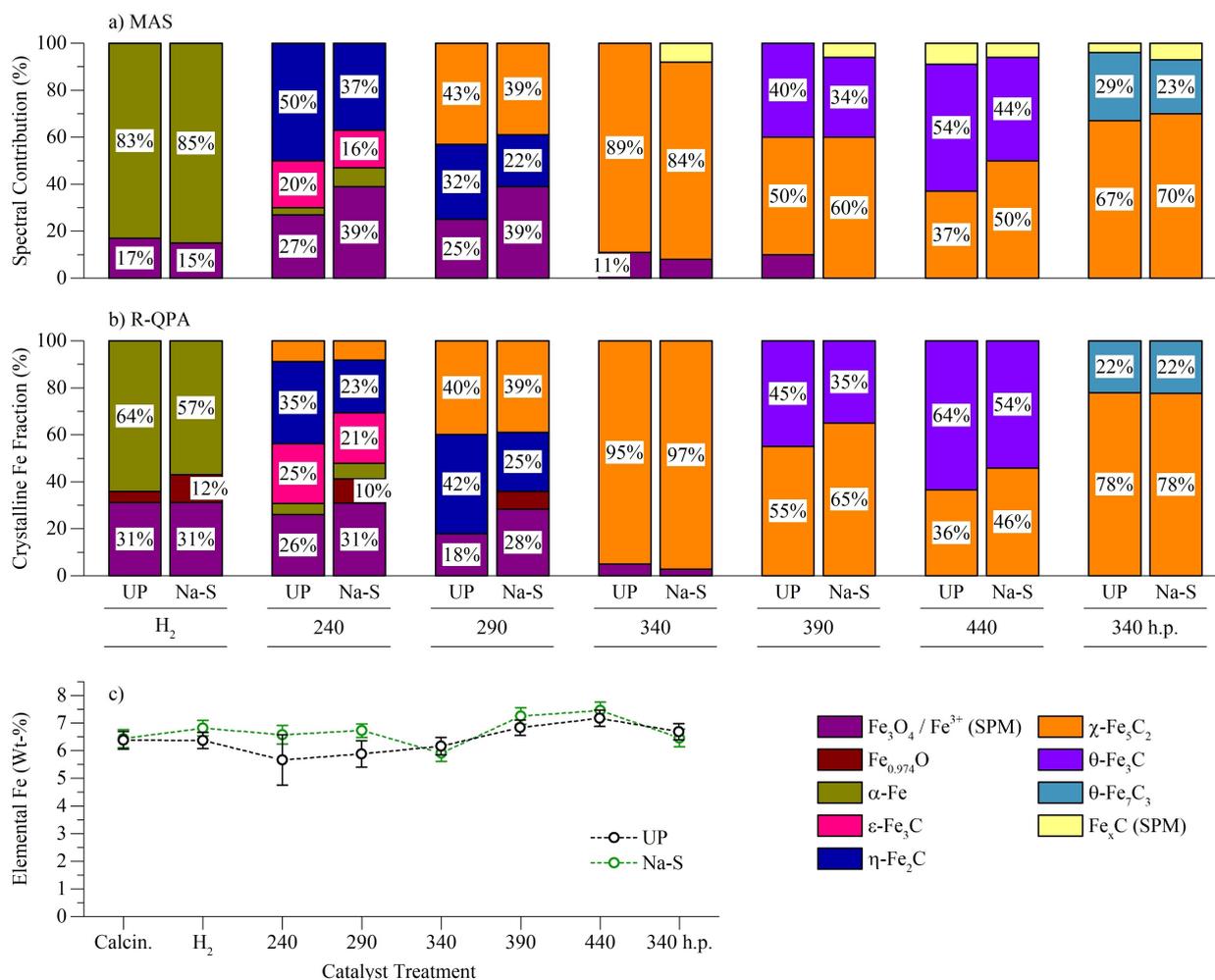
ChemCatChem

Full Papers
doi.org/10.1002/cctc.202000707

**Chemistry
Europe**
European Chemical
Societies Publishing

Figure 5. Fe phase quantifications for UP and Na–S (Fe(–Na–S)/α-Al$_2$O$_3$) catalyst materials after the applied catalyst treatments. Quantification results for a) room temperature (300 K) Mössbauer Absorption Spectroscopy (MAS), and b) Rietveld Quantitative Phase Analysis (R-QPA). R-QPA results were used to derive c) the elemental Fe wt-% loadings from the crystalline Fe phases. Percentage labels cut-off is set to < 10%. SPM = superparamagnetic.

the re-reduction of any re-oxidized α-Fe.[55] Therefore, the overall carburization extent increases as is observed. Furthermore, the increase in the carbon deposition by the Boudouard reaction at temperatures ≳ 300 °C (Figure S6),[20,64–67] likely decreases the Fe phases propensity for re-oxidation upon exposure to air.

Fe Carbide Formation below ≈ 300 °C

After the mildest CO carburization treatment 240, ε-Fe$_3$C and η-Fe$_2$C are the major Fe carbide phases formed within the catalysts (Figure 5a–b). Small amounts of residual α-Fe can be detected as a sign of incomplete carburization for both the UP and Na–S 240 catalyst materials. With R-QPA, also small amounts of χ-Fe$_5$C$_2$ (8–9%) after the catalyst treatment 240 could be quantified (Figure 5b). MAS did not quantify any of the χ-Fe$_5$C$_2$ phase for either the UP or the Na–S catalyst materials (Figure 5a). In the XRPD patterns for the 240 catalysts,

weak diffraction peaks originating from the χ-Fe$_5$C$_2$ phase can be seen, perhaps best, from the two small peaks at ≈ 21.3° and ≈ 22.5° 2θ (Figure 2a and Figure 3a).

With further increasing the catalyst CO carburization time and temperature with the catalyst treatment 290, the χ-Fe$_5$C$_2$ phase contribution increases. At the same time, the η-Fe$_2$C phase is still present, while the ε-Fe$_3$C phase is no longer observed with either R-QPA or MAS (Figure 5a–b).

The ε-Fe$_3$C phase is expected to form within a carburization the temperature range of 100–265 °C,[34,35,38,50,68–71] and the η-Fe$_2$C phase between 160–300 °C.[4,23,34–36,38,69–72] Thus, the R-QPA and MAS quantification results with respect to the ε-Fe$_3$C and η-Fe$_2$C phases are in good agreement with the literature. Furthermore, in literature, the formation of the χ-Fe$_5$C$_2$ phase has been observed to start, with α-Fe as the starting material, from temperatures of ≈ 250–260 °C.[68,69,73] As a notable discrepancy, Niemantsverdriet et al. have observed the formation of the χ-Fe$_5$C$_2$ phase to already start from a temperature of 190 °C.[4] This temperature is a lot lower than expected, based

ChemCatChem

Full Papers
doi.org/10.1002/cctc.202000707

**Chemistry
Europe**
European Chemical
Societies Publishing

on both the R-QPA and MAS quantifications (Figure 5a–b) and the literature.

With the use of MAS, Niemantsverdriet et al. observed the formation of Fe carbides from α-Fe under H_2:CO 1:1 at 1 bar as: at 190 °C (24 h) unknown quantity of η-Fe_2C and 36% χ-Fe_5C_2, at 240 °C (24 h) 35% η-Fe_2C and 65% χ-Fe_5C_2, at 350 °C (3 h) 12% η-Fe_2C, 47% χ-Fe_5C_2 and 41% θ-Fe_3C and at 450 °C (1.5 h) 100% θ-Fe_3C.[4] When comparing the results by Niemantsverdriet et al. to the quantification results for the Fe carbides in Figure 5a–b, it can observed that the results by Niemantsverdriet et al. would compare more reasonably, if a constant temperature shift of $\approx +50$ °C is applied to their data.

With FTS reaction under H_2:CO 2:1 at 1.03 bar at 200 °C (3.9 h) Boellaard, van der Kraan and Geus,[34] quantified Fe carbides with MAS as 18% ε-Fe_3C and 54% η-Fe_2C. No observation of the χ-Fe_5C_2 phase was made. In a similar manner, with MAS quantification, Amelse et al. observed only the ε-Fe_3C and η-Fe_2C phases after exposing α-Fe to H_2:CO 3:1 at 250 °C (2.5 h) at atmospheric pressure, without observing any presence of the χ-Fe_5C_2 phase.[50] At higher carburization temperatures, Jiang et al. have quantified with MAS 14% Fe_3O_4, 25% η-Fe_2C and 61% χ-Fe_5C_2 after H_2:CO 1:1 at 10 bar at 300 °C (50 h) with pre-reduced K-promoted Fe catalysts.[72] The results at 240 °C (24 h) by Niemantsverdriet et al. seem very similar to the results by Jiang et al. at 300 °C (50 h), and are the best match to the R-QPA and MAS results with the catalyst treatment 290 (CO, 290 °C, 3 h) (Figure 5a–b).

Thus, we postulate that there should be a temperature offset of $+50$ °C to all of the results by Niemantsverdriet et al.,[4] after which their quantifications are in a good agreement with the R-QPA and MAS results reported in Figure 5a–b, and also with those in the above mentioned literature studies.

The exception in the results by Niemantsverdriet et al. in comparison to the R-QPA and MAS quantifications in Figure 5a–b, is that even with the $+50$ °C shift some η-Fe_2C (12%) should be present even after carburizing reaction at 400 °C (3 h). Furthermore, Wezendonk et al. have observed the η-Fe_2C phase at 340 °C (≥ 24 h) in their Fe carburization and FTS reaction studies.[16] We could not observe any η-Fe_2C with ≥ 340 °C CO carburization temperature, i.e. with the catalyst treatments 340–440. The common denominator for both of the cited studies is that the η-Fe_2C phase is *preformed* first at a lower carburization temperature and then heated subsequently to a higher reaction temperature. Thus, if a η-Fe_2C phase is present a priori to the FTS reaction, some of it *may remain stable* i.e. its carbide-to-carbide transition is hindered with reaction temperatures higher than 300 °C. However, on the basis of the quantification results in Figure 5a–b we can state that the *η-Fe_2C phase does not directly form at 340 °C* when α-Fe is used as the starting phase for the carburization.

Thus, we propose the temperature window 160–300 °C as the formation temperature for the η-Fe_2C phase from α-Fe. Nonetheless, a maximum thermal stability of the phase can reach at least ≈ 340 °C if the η-Fe_2C phase is preformed prior to the temperature increase. We acknowledge, but exclude the rather high 400 °C maximum thermal stability for the η-Fe_2C

phase, as observed by Niemantsverdriet et al. for now, due to possible uncertainty in their reaction temperature.

Fe Carbide Formation above ≈ 300 °C

With increasing severity of the CO carburization with treatments 340, 390, and 440, only the χ-Fe_5C_2 and θ-Fe_3C phases are observed as Fe carbides with both R-QPA and MAS quantifications (Figure 5a–b). Some SPM, poorly crystalline Fe_xC phases are also observed with MAS quantifications after the higher temperature catalyst carburization treatments (Figure 5a). These phases are not observable with XRPD-based R-QPA (Figure 5b). The poorly crystalline Fe_xC phases could perhaps be related to intergrowth structures of the χ-Fe_5C_2 and θ-Fe_3C phases.[74–76] After the catalyst treatment 340, only the χ-Fe_5C_2 phase is observed as the sole carbide phase and the treatment 340 is the only one to form a near pure, single Fe carbide phase catalyst. Both R-QPA and MAS agree on the quantification (Figure 5a–b), and the XRPD patterns do not show any unassigned diffraction peaks (Figure 2c and Figure 3c). The expected formation temperature range for the χ-Fe_5C_2 phase is about 250–400 °C as based on the experimental literature observations.[8,19,26,50,68–70,72,73,77]

With both R-QPA and MAS quantifications, the formation of the χ-Fe_5C_2 phase from α-Fe is still observed with the catalyst treatment 440. Figure 5a–b shows that the χ-Fe_5C_2 phase forms at a temperature as high as 440 °C with 16 h of CO exposure time. This temperature is $\approx +40$ °C higher than the highest temperatures observed in literature for the formation of the χ-Fe_5C_2 phase. Nagakura observed the preservation of the χ-Fe_5C_2 phase after heating their precursor carbide at 400 °C for 0.1 h.[68] With the assumption of the previously discussed $+50$ °C temperature shift, 400 °C is also the highest observation temperature for the χ-Fe_5C_2 phase by Niemantsverdriet et al.[4]

By analyzing the X-ray diffraction patterns of Figure 2c–d and Figure 3c–d, the increasing amount of the θ-Fe_3C phase overlaps with the X-ray diffraction from the most intense peaks of the χ-Fe_5C_2 phase, obfuscating its presence. Nevertheless, the weak X-ray diffraction peaks located at around 21.3° 2θ and 22.5° 2θ, originating from the χ-Fe_5C_2 phase, make the presence of the phase clear in the XRPD patterns even after the catalyst treatment 440 (Figure 2e and Figure 3e). The mentioned χ-Fe_5C_2 phase diffraction peak obfuscating effects in relation to the presence of the θ-Fe_3C phase might explain the lack of literature observations for the χ-Fe_5C_2 phase up to temperature of 440 °C, at least for the diffraction-based characterization methods.

The presence of the θ-Fe_3C phase is expected within the temperature range of 310–600 °C based on literature data.[4,27,68,78] However, we could not observe any presence of the θ-Fe_3C phase in the catalyst materials with carburization treatment temperatures below 390 °C.

The lowest observation temperatures for the θ-Fe_3C phase from gas phase carburizations are by Nagakura with 350 °C,[68] and Shultz et al. with 310 °C.[27] Furthermore, in martensite tempering studies, the formation of the θ-Fe_3C phase as low as

ChemCatChem

Full Papers
doi.org/10.1002/cctc.202000707

**Chemistry
Europe**

European Chemical
Societies Publishing

250–267 °C has been observed.[38,74] These formation temperatures for the θ-Fe₃C phase in the martensite tempering studies seem very low in comparison to other literature, and disagree with the R-QPA and MAS quantification results shown Figure 5a–b. They are thus excluded from further discussion.

Observations on the formation of the θ-Fe₃C phase after carburizing polycrystalline α-Fe film with CO at 350 °C (3 h) have been made by Nagakura, with the use of Electron Diffraction (ED).[68] The closest carburization conditions corresponding to Nagakura's reaction conditions are with the catalyst treatment 340, with which we could not form any observable amounts of θ-Fe₃C using the applied bulk characterization techniques (Figure 5a–b). That is, Nagakura's observations at 350 °C could be very close to the precise lower temperature limit for the θ-Fe₃C formation.

With regard to the observations with XRPD by Shultz et al. on formation of θ-Fe₃C from α-Fe under H₂:CO 2:1 at 310 °C (6 h),[27] no imminently clear explanation can be given for the deviation to the R-QPA and MAS Fe quantification results. However, possibly, in the study by Shultz et al., the α-Fe was exposed to the carburizing H₂:CO gas mixture *directly* at 310 °C, which might have caused significant reactor bed heating as the exothermic FTS reaction is initiated.[56] This idea would be supported by an another experiment by Shultz et al. in the same publication, where by step-wise increasing the CO exposure temperature from 150 °C to 350 °C on the α-Fe starting material, only the χ-Fe₅C₂ phase was formed.[27] This result by Shultz et al. would be in close agreement with the results in Figure 5a–b. Thus, we assume that the actual, efficient reactor bed temperature has been a lot higher than 310 °C in the discussed experiment by Shultz et al.[27] Therefore, the 310 °C data point is ignored from the expected low-end formation temperature for the θ-Fe₃C phase.

We did not test for the high-end temperature limit for the θ-Fe₃C phase formation or stability. With gas phase carburizations at 500 °C, Shultz et al. observed θ-Fe₃C with 6 h carburiza-

tion of α-Fe with CH₄,[27] while also under H₂:CO (1.5 h),[4] and CO (1 h),[68] the θ-Fe₃C phase has been detected. Jozwiak et al. reduced the α-Fe₂O₃ phase with CO to α-Fe at 500 °C *without* formation of the θ-Fe₃C phase.[55]

By heat treating the preformed θ-Fe₃C phase, Wood et al. have observed an initial slow, at 377 °C, and rapid decomposition of θ-Fe₃C to α-Fe above 527 °C.[79] Other authors have still observed the θ-Fe₃C phase after heating their catalysts between 525–550 °C.[68,78] The highest stability temperature for the θ-Fe₃C phase has been observed by Nagakura, who observed the θ-Fe₃C phase even after heating a preformed Fe carbide for 16 h in vacuum at 600 °C.[68] Podgurski et al. have noted that decomposition of "a high temperature carbide", most likely θ-Fe₃C, to α-Fe takes place at 500 °C. If a Fe particle surface oxide was formed e.g. possibly when CO is used as a carburizing agent in comparison to O-free hydrocarbons, the decomposition temperature of the carbide to α-Fe was increased.[56]

Thus, the higher-end stability temperature of the θ-Fe₃C phase is dependent on how easily the C atoms can be expulsed from the θ-Fe₃C lattice, allowing the carbide phase to decompose to α-Fe and C atoms. Thus, the presence or absence of carbide decomposition inhibiting shell oxide layers on the θ-Fe₃C phase can be used to explain the discussed differences in the θ-Fe₃C phase stability between 500–600 °C.

Finally, based on the R-QPA and MAS quantifications (Figure 5a–b) and the discussion on the literature observations, we assign the formation temperature range for the θ-Fe₃C phase as 350–500 °C. A preformed θ-Fe₃C phase can be stable up to 600 °C if C atom expulsion from the θ-Fe₃C lattice is hindered due to a Fe oxide layer.[56] Without the Fe oxide layer, the θ-Fe₃C phase decomposes readily into α-Fe and C species above 527 °C.[79]

The Fe carbide formation temperature regions have been updated from the purely literature based observations of noninterpreted data points in reference [2] to the Figure 6 to
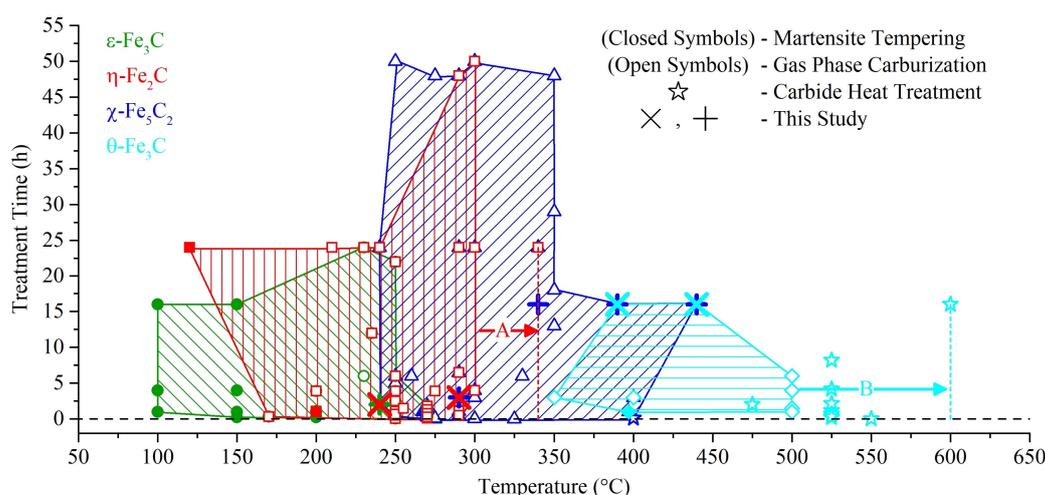

Figure 6. Fe carbide formation regions (*hatched fill*) as temperature versus treatment exposure time as based on the available experimental literature data and this study. *Arrows:* Maximum thermal stability with preformed Fe carbides for (A) η-Fe₂C and (B) θ-Fe₃C. Formation temperatures for the θ-Fe₇C₃ phase are excluded. Figure is modified from reference.[2]

follow the presented results and discussion (Figure 5a–b). The rejected data points and the $+50\,°C$ shift to the reaction temperatures in the data by Niemantsverdriet et al.,[4] have also been included in the updated Figure 6.

Figure 6 only contains data points from studies where the carburization starting material has been either α-Fe or martensite,[2] as in this study (excluding treatment 340 h.p.). This is needed in order to decouple Fe reduction from Fe carburization effects.[2] An example of perceived shifts to Fe carbide formation temperatures due to Fe reduction effects is given later in this text. Furthermore, the data points in Figure 6 are from different studies where different catalysts systems have been used.[2] No obvious correlation between any particular catalyst preparation method, or type, and Fe carbide formation is conceivable from the studies.

The updated Fe carbide formation temperature regions are, as shown in Figure 7, as follows: ε-Fe$_3$C (100–265 °C), η-Fe$_2$C (160–300 °C), χ-Fe$_5$C$_2$ (240–420 °C) and θ-Fe$_3$C (350-500 °C), when compared at 5 h treatment time in the Figure 6. Furthermore, the χ-Fe$_5$C$_2$ high-end formation temperature can be as high as 440 °C after a longer, 16 h CO carburization time. The preformed η-Fe$_2$C and θ-Fe$_3$C phases can be stable up to $\approx 340\,°C$ and $\approx 600\,°C$, respectively, but do not directly form at these temperatures from α-Fe.

As a final note on the Fe carbide formation temperatures: for the formation of the ε-Fe$_3$C phase within the temperature range of ≈ 100–160 °C, the synthesis route will likely need to go via martensite tempering (Figure 6). At these very low carburization temperatures CO adsorption/dissociation products do not necessarily desorb,[80] likely inhibiting α-Fe carburization via a gas phase CO.[15,81]

Effect of Na-S Promotion

When comparing the UP and Na—S catalysts for the formation of various Fe carbides with the catalyst treatments 240–440 it can be noted that the relative formation quantities for the different Fe carbides from α-Fe are not affected by the added Na—S promotion in any major way (Figure 5a–b).

Significant effects from the Na—S promotion on α-Fe carburization are, as shown in Figure 5, as follows: i) an increased Fe oxide contribution with treatments 240 and 290 and ii) Na—S promotion seems to increase the χ-Fe$_5$C$_2$ phase content at the expense of the θ-Fe$_3$C phase with treatments 390 and 440. In the MAS observations, a non-SPM (i.e., larger

crystallite diameter) Fe phase with Fe^{3+} appeared after applying catalyst treatments 240 and 290 with the addition of the Na—S promotion (Table S2).

The increased Fe oxide contribution with Na—S 240 and Na—S 290 catalysts in relation to the respective UP catalyst is in agreement with both the R-QPA and MAS quantifications (Figure 5a–b). Addition of alkali in general decreases the reducibility of Fe oxides by H$_2$,[30,49,82] possibly by stabilizing the oxides.[49] Together with the earlier discussion on the possible oxidative effects due to the O atoms from CO dissociation, we thus assign the increased Fe oxidation with Na—S 240 and Na—S 290 catalysts to the increased stability for Fe oxide formation. From the treatment 340 upwards towards higher carburization temperatures and times, the Na—S effect is absent as the gas environment becomes more reducing with CO (and H$_2$).[55] The increased carburization/reduction temperature likely overcomes the possibly increased Fe oxide stability.

Regarding the relative stabilities of the χ-Fe$_5$C$_2$ and θ-Fe$_3$C phases, the Na—S promotion stabilizes the χ-Fe$_5$C$_2$, while decreasing the presence of the θ-Fe$_3$C phase with the high temperature catalyst treatments 390 and 440 (Figure 5a–b). In the R-QPA quantifications, the χ-Fe$_5$C$_2$ phase amount is increased $\approx +10\%$ in the Na—S catalyst materials after the treatments 390 and 440 at the expense of the θ-Fe$_3$C phase. The MAS quantifications also agree with the trend of the decreased θ-Fe$_3$C phase content after these catalyst treatments.

As further effects on the Na—S promotion in Fe carburization, it can be mentioned that occasionally in literature the addition of alkali has been cited to increase the carburization of Fe catalysts, but the R-QPA and MAS results do not agree with this observation (Figure 5a–b). The observed differences can be explained with the starting Fe phase for the carburization, i.e. whether the carburization process is started with α-Fe or a Fe oxide. For example, Berry and Smith have observed, with MAS, that the added alkali K promotion aids in the carburization of the starting α-Fe$_2$O$_3$ material.[83] Under pure CO at 270 °C after 12 h of CO exposure time, the added alkali K enhanced the Fe carbide formation from the α-Fe$_2$O$_3$ starting material in comparison to the unpromoted catalyst. Interestingly, with a short CO exposure time of 2 h at 270 °C regardless of the K promotion, the authors observed that only Fe$_3$O$_4$ formed without any Fe carbides. The dependency of the extent of carburization on the CO exposure time would also explain the previously discussed increased Fe oxidation with Na—S 240 and Na—S 290 catalysts with the short exposure times (≤ 3 h) (Figure 5a–b). The increased CO carburization rate of α-Fe$_2$O$_3$
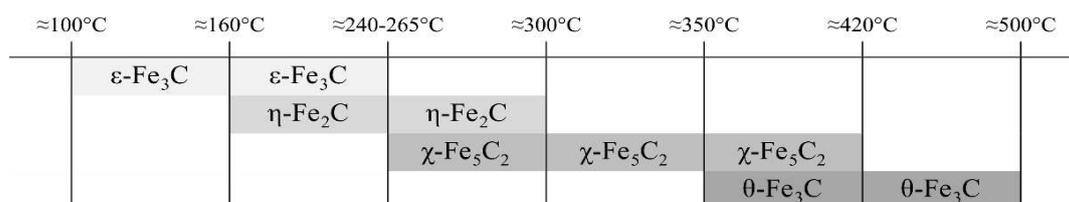
$\approx 100\,°C$	$\approx 160\,°C$	≈ 240-265 °C	$\approx 300\,°C$	$\approx 350\,°C$	$\approx 420\,°C$	$\approx 500\,°C$
ε-Fe$_3$C	ε-Fe$_3$C					
	η-Fe$_2$C	η-Fe$_2$C				
		χ-Fe$_5$C$_2$	χ-Fe$_5$C$_2$	χ-Fe$_5$C$_2$		
				θ-Fe$_3$C	θ-Fe$_3$C	

Figure 7. Fe carbide formation temperature ranges as estimated from the Figure 6 at 5 h treatment time. The θ-Fe$_7$C$_3$ phase is excluded as its formation is a more complex, not a solely temperature dependent, phenomenon.

ChemCatChem

Full Papers
doi.org/10.1002/cctc.202000707

Chemistry
Europe
European Chemical
Societies Publishing

starting materials due to the alkali promotion has been also observed by Ribeiro et al.,[84] and also can be seen in the MAS quantification results by O'Brien et al.[30] and Bukur et al.[61]

The addition of alkali (as Na or K) promotes the CO_2 releasing Water-gas Shift (WGS) reaction with Fe catalysts.[57,85,86] The addition of alkali has been observed to increase the exchangeability of surface O atoms with CO on K-promoted Al_2O_3, especially at lower temperatures of $\approx 300\,°C$.[87] Also, an increase in the rate of the WGS reaction with the same transition metal-free K/Al_2O_3 catalyst material has been observed.[88] It was found that the addition of alkali seems to enhance the interaction of CO with the catalyst surface O atoms, while also increasing the WGS reaction rate. The enhanced O/CO interaction could also suggest a possibility for improved Fe oxide reduction by CO in the presence of alkali. Effectively then, according to the presented discussion, with the added alkali to a Fe oxide, the Fe oxide's reducibility to zerovalent Fe should be i) increased at low temperatures ($\approx 300\,°C$) with CO as the reductant when a sufficiently long CO exposure time ($> 3\,h$) has been applied,[30,83,87] and ii) decreased with H_2 due to Fe oxide stabilization by the alkali.[30,49,82]

Indeed, in a XRPD study where a precursor α-Fe_2O_3 was carburized directly with i) pure CO or, ii) a H_2:CO 100:1 mixture, the Fe reduction steps for the α-Fe_2O_3 were modified.[5] As reading from the XRPD patterns in the study; the Fe reduction steps can be seen to shift for α-$Fe_2O_3 \rightarrow Fe_3O_4$ ($\approx +35\,°C$), $Fe_3O_4 \rightarrow Fe_xO$ (wüstite) ($\approx +65\,°C$) and $Fe_xO \rightarrow Fe_xC$ (i.e., α-Fe) ($\approx +93\,°C$) when switching the carburizing gas from pure CO to a 100:1 H_2:CO mixture. That is, the α-Fe_2O_3 was more poorly reducible with the 100:1 H_2:CO mixture than with pure CO. Noteworthy is that in the study, the used α-Fe_2O_3 catalysts were prepared using Na_2CO_3 as the precipitation agent, which, despite a washing,[89] is likely to leave residual Na in the catalyst with sufficient concentration to act as a promoter. Furthermore, X-ray Fluorescence (XRF) was used to evaluate the catalyst material purity, a technique which detects the Na elements poorly.[90] The inadvertent Na promotion would explain both; i.e., the more efficient reduction of the Fe oxides at lower temperatures by CO as discussed, and the observations on the Fe_xO (wüstite) phase during Fe reduction step.[49,55]

Therefore, taking everything into account, the increased carburization of alkali-promoted Fe oxides can be explained with a more efficient Fe oxide reduction to α-Fe with CO. α-Fe then subsequently carburizes to Fe carbides with the available CO. In other words, *the Fe reduction step to α-Fe is enhanced by alkali, not the carburization step* when starting with a Fe oxide material under a carburizing atmosphere. This explains the lack of significant Na(–S) effect in the results on the α-Fe carburization with the applied CO treatments 240–440 (Figure 5a–b).

Formation of the θ-Fe_7C_3 Phase

Low yet clearly observable amounts of 22–29% of the θ-Fe_7C_3 phase were formed after the catalyst treatments 340 h.p. (Figure 5a–b). With these treatments, the α-Fe_2O_3 phase was

used as the carburization starting Fe phase, directly for the carburization reaction at 25 bar CO pressure at $340\,°C$. The addition of the Na–S promotion did not affect the formation of the θ-Fe_7C_3 phase. This while minding for the differences in the applied CO exposure times of $120\,h$ for the UP and $168\,h$ for the Na–S 340 h.p. catalyst materials. The θ-Fe_7C_3 phase can be formed under rather extreme conditions,[91–94] but may also form under milder FTS reaction conditions, which are more relevant to the present discussion.[20,28,95] In order to form the θ-Fe_7C_3 phase under mild conditions, Tajima and Hirano used a Ba-promoted Fe_3O_4 carburized with pure CO under unspecified pressure at $300–375\,°C$.[28] Audier, Bowen and Jones were able to prepare single crystals of θ-Fe_7C_3 from α-Fe under CO:CO_2 3:1 at $500\,°C$,[95] with undefined, yet presumably, at atmospheric pressure. As Audier, Bowen and Jones were able to prepare the θ-Fe_7C_3 phase without a Fe oxide, Ba promotion or high CO pressure; the results suggest that the common required factor for preparing the θ-Fe_7C_3 phase is none of the mentioned parameters. A common factor for mild condition preparation of the θ-Fe_7C_3 phase might be the CO_2 as Audier, Bowen and Jones used CO_2 in their carburizing gas mixture.[95] In the study by Tajima and Hirano,[28] perhaps, the role of Ba has been to aid the Fe oxide reduction by CO, akin to the earlier discussed alkali effect, releasing CO_2 in the reduction process. Ba promotes Fe oxides towards the WGS reaction,[86,96,97] suggesting similar expected behavior for Ba promotion as for the earlier discussed alkali WGS promotion effect.

At Sasol, the formation of the θ-Fe_7C_3 phase has been observed at higher pressure (> 60 bar) under industrial FTS reaction conditions in end-of-life catalysts.[20] The Fe-based FTS catalysts have the tendency to re-oxidize to WGS catalyzing Fe_3O_4 over time.[20,26,59,60,86,98,99] The catalyst re-oxidation could explain the formation of the θ-Fe_7C_3 phase at later stages of the catalyst life-time at Sasol along the WGS catalyzing Fe_3O_4,[20] as the WGS reaction releases CO_2.[86,98]

The formation of the θ-Fe_7C_3 phase with catalyst treatment 340 h.p. might then be explained with the increased concentration of CO_2 in the carburizing gas stream, due to the reduction of the Fe oxide with CO.[55] Perhaps, with the elevated CO pressure, the rate of the initial Fe oxide reduction is momentaneously sufficiently high for increasing the CO_2 concentration and thus allowing the θ-Fe_7C_3 formation, irrespective of the added Na–S promotion. The formed quantity of the θ-Fe_7C_3 phase was not affected by the different carburization times (Figure 5a–b), i.e. $168\,h$ for UP as opposed to $120\,h$ for Na–S catalysts with the catalyst treatment 340 h.p. This would suggest that the formation of the θ-Fe_7C_3 phase does not take place during the steady state of the applied treatments, but perhaps, during the temperature ramp or early period of the catalyst treatment. This is also when then CO_2 concentration in the carburizing gas stream would be expected to be the highest due to the Fe oxide reduction. As the carbon deposition rates between the catalyst treatments 340 and 340 h.p. are very similar Figure S6, the deposited carbon from the Boudouard reaction probably does not play a major role in the formation of the θ-Fe_7C_3 phase. Thus, we speculate that the θ-Fe_7C_3 formation is dependent on the presence of CO_2 in the

gas mixture during the gas phase carburization. However, more research on this topic should be performed by systematically carburizing α-Fe and Fe oxides with different $CO:CO_2$ mixtures. This might reveal whether a CO_2 correlation to the θ-Fe_7C_3 formation exists.

Solely based on the R-QPA and MAS quantifications in Figure 5a–b, the formation temperature ranges for the θ-Fe_7C_3 phase cannot be deduced. However, according to Tajima and Hirano, the θ-Fe_7C_3 phase is only stable within the temperature range 300–375 °C.[28] This temperature range is in agreement with the observation of the θ-Fe_7C_3 phase forming with the catalyst treatment 340 h.p. at 340 °C (Figure 5a–b). The higher end temperature stability of the θ-Fe_7C_3 phase might be dependent on the purity of the carbide phase.[94] An oxygen-free θ-Fe_7C_3 phase has been witnessed to survive temperatures up to ≈400–500 °C before decomposing into α-Fe and C atoms.[94]

Assignment of Fe Carbide Properties with X-ray Powder Diffractometry/Rietveld Quantitative Phase Analysis and Mössbauer Absorption Spectroscopy

Figure 5a–b shows that the experimental MAS and XRPD based R-QPA quantifications are very much in line with each other and the R-QPA fittings to the measured diffractograms correspond well with the employed Fe carbide crystal structures, as can be seen in Figure 2 for UP and in Figure 3 for Na–S catalysts. It is therefore safe to conclude that the earlier identification and proposed nomenclature for the Fe carbides followed here is a reasonable one.[2] In other words, the Fe carbides encountered in FTS research can be identified as ε-Fe_3C, η-Fe_2C, χ-Fe_5C_2, θ-Fe_3C and θ-Fe_7C_3, with the lattice parameters and the crystal structures by the listed authors in Table 2.

The use of the inaccurate nomenclature of assigning any of the Fe carbides as pseudo-hexagonal, "ε-carbides", (ε-)Fe_2C or ε'-$Fe_{2.2}C$ is discouraged for the time being. At the moment, no known and unique crystal structures can be associated to such Fe carbide labels.[2] In-depth discussion on the FTS reaction related Fe carbide crystal structures and their labelling is presented in reference [2] and the discussion is not repeated here.

Fe Carbide Lattice Parameters and Hyperfine Fields

The R-QPA fitted and averaged Fe carbide lattice parameters, for all the observations per Fe carbide phase, are given in Table 2, while the individual lattice parameters are shown in Figures S9 and S10. The averaged MAS-based Fe hyperfine fields and relative fitted spectral contribution derived non-equivalent Fe site ratios are shown in Table 3 for the Fe carbides. The reference MAS values from experimental literature studies in Table 3 are reproduced from reference.[2] Na–S promotion did not have any significant effect, on either the fitted Fe carbide lattice parameters or the hyperfine fields.

The mean values of the lattice parameters used for the R-QPA fits, tabulated in Table 2, are in general in good agreement with the lattice parameters reported in literature. Especially noteworthy is the good agreement of the η-Fe_2C phase to the proposed unit cell translation by Hirotsu and Nagakura for "(pseudo-)hexagonal" Fe carbide observed by Barton and Gale.[11,23,24]

Table 2. Averaged Fe carbide lattice parameters and crystal structures used in the Rietveld Quantitative Phase Analysis (R-QPA) with comparisons to the lattice parameters by the crystal structures' authors.

Fe Carbide Phase	Space Group		Lattice Parameters Author [Å]	This Study[a] [Å]	Database Number ICDD-PDF-4+ (2016)	Author
ε-Fe_3C	Hexagonal, P6₃22 (182)	a	4.767	4.76±0.00	04-008-9572	Nagakura (1959) [68]
		b	4.767	4.76±0.00		
		c	4.354	4.36±0.00		
η-Fe_2C[b]	Orthorhombic, Pnnm (58)	a	4.862	4.84±0.01	04-013-9510	Hirotsu (1972) [23]
		b	4.360	4.35±0.00		
		c	2.755	2.76±0.00		
χ-Fe_5C_2	Monoclinic, C2/c (15)	a	11.588	11.56±0.01	00-051-0997	Retief (1999) [14]
		b	4.579	4.57±0.01		
		c	5.059	5.07±0.00		
χ-Fe_5C_2 (h.p.)[c]	Monoclinic, C2/c (15)	a	–	11.61±0.01	–	–
		b	–	4.57±0.00		
		c	–	5.04±0.00		
θ-Fe_3C[d]	Orthorhombic, Pnma (62)	a	5.081	5.07±0.00	9014027[e]	Wood (2004) [79]
		b	6.754	6.76±0.02		
		c	4.515	4.53±0.01		
θ-Fe_7C_3[d]	Orthorhombic, Pnma (62)	a	4.540	4.52±0.00	04-002-8165	Fruchart (1965)[f] [100]
		b	6.879	6.90±0.01		
		c	11.942	11.91±0.00		

[a] The mean values over all observations of the Fe carbide phase with Standard Deviations (STDs), [b] The author's lattice parameters are translated, according to Hirotsu and Nagakura [24], to correspond to the Fe carbide observed by Barton and Gale [11], [c] Formed from Fe oxide precursor (α-Fe_2O_3/α-Al_2O_3) with the catalyst treatment 340 h.p, [d] Diffraction peak overlap with χ-Fe_5C_2 or χ-Fe_5C_2 (h.p.) causes inaccuracy on the lattice parameters, [e] Crystallography Open Database (COD) number, [f] The original article written in French by Fruchart et al. is not readily available, but some discussion on the crystal lattice can be found in publication by Audier, Bowen and Jones.[95]

ChemCatChem

Full Papers
doi.org/10.1002/cctc.202000707

Chemistry
Europe
European Chemical
Societies Publishing

Table 3. The averaged Mössbauer Absorption Spectroscopy (MAS) spectral contribution derived relative ratios for non-equivalent Fe positions and hyperfine fields per Fe carbide. Averaged, experimental literature values are also provided for comparison from reference [2].

Fe Carbide Phase	Space Group	Non-equivalent Fe Positions			Hyperfine Field (at room temperature)	
		Tot. Count[a]	Rel. Ratio Nominal[c]	Fitted[d]	Literature [T]	This Study[b] [T]
ε-Fe₃C	Hexagonal, P6₃22 (182)	1	1	1	24.5 ± 0.8	23.4 ± 0.3
η-Fe₂C	Orthorhombic, Pnnm (58)	1	1	1	17.2 ± 0.3	17.3 ± 0.3
χ-Fe₅C₂	Monoclinic, C2/c (15)	3	2	1.9 ± 0.3	21.4 ± 0.3	21.4 ± 0.3
			2	1.8 ± 0.3	18.1 ± 0.4	18.7 ± 0.3
			1	1.0 ± 0.0	10.9 ± 0.9	11.4 ± 0.3
χ-Fe₅C₂ (h.p.)[e]	Monoclinic, C2/c (15)	3	2	1.3 ± 0.0	–	21.5 ± 0.1
			2	1.2 ± 0.0	–	18.0 ± 0.1
			1	1.0 ± 0.0	–	10.3 ± 0.1
θ-Fe₃C	Orthorhombic, Pnma (62)	2	(2)	–	20.8 ± 0.3	–
			(1)	–	20.0 ± 0.3	–
			Avg.[f]	1	20.8 ± 0.5	20.5 ± 0.3
θ-Fe₇C₃	Orthorhombic, Pnma (62)	5	(1)	1.0 ± 0.0	22.9 ± 0.1	22.4 ± 0.1
			(2)	–	(–)[g]	–
			(1)	0.9 ± 0.3	18.5 ± 0.1	19.5 ± 0.4
			(2)	1.8 ± 0.3	16.3 ± 0.1	16.3 ± 0.1
			(1)	–	(21.0)[g]	–

[a] Determined based on the crystal structures from authors in Table 2, [b] Mean values over all observations of the phase with the Standard Deviations (STDs), [c] Nominal ratios assigned per experimental MAS data, where assignments in parenthesis () are uncertain, [d] Averaged ratios derived from the spectral contributions per fitted hyperfine field, [e] Formed from Fe oxide precursor (α-Fe₂O₃/α-Al₂O₃) with the treatment 340 h.p., [f] Commonly, an averaged hyperfine field is fitted for the θ-Fe₃C in the experimental literature data, [g] Uncertain assignments values.

The most significant deviations from the authors' unit cells are with the χ-Fe₅C₂ and θ-Fe₇C₃ phases. Especially noteworthy is the distinctively distorted χ-Fe₅C₂ (h.p.) phase formed with the catalyst treatment 340 h.p., in both the UP and Na–S catalysts. The θ-Fe₃C phases' mean lattice parameters have large STDs complicating discussion on the phase's parameters (Table 2). The MAS hyperfine fields for the ε-Fe₃C, η-Fe₂C, χ-Fe₅C₂ and θ-Fe₃C phases are in good agreement with the expected experimental values interpreted from literature (Table 3).[2]

The hyperfine field associable to the ε-Fe₃C phase and centered around 24.5 T exhibits a rather large STD of ±0.8 in the literature reference value (Table 3).[2] The reference value is collected by Le Caër et al. and the observations range from 23.2 to 26.2 T.[7] This wide hyperfine field range was speculated to be due to possibly different (than C) alloying elements, particle sizes and/or C content in the Fe carbide lattices.[7] In this study, the ε-Fe₃C is at the lower end of the hyperfine field range (23.4 ± 0.3 T, Table 3). This could indicate increased C content in the lattice. The C contents for the Fe carbides are discussed more later on in the text.

For the θ-Fe₃C phase, two Fe hyperfine fields should be assigned for each of the non-equivalent Fe positions (Table 3). However, as the MAS hyperfine fields are close to each other, therefore commonly a single averaged field is used.

The distinctively distorted unit cell for the χ-Fe₅C₂ (h.p.) phase is formed after the catalyst treatment 340 h.p. By comparing the Rietveld method calculated χ-Fe₅C₂ phase diffraction patterns (Figure 2b–e and Figure 3b–e) to the χ-Fe₅C₂ (h.p.)'s calculated phase pattern after the high-pressure

treatment (Figure 2f and Figure 3f), a shift towards lower 2θ in the most intense diffraction peak can be observed. The shift towards lower 2θ signifies increase in, at least one, unit cell lattice parameter for the diffracting phase. Indeed, the χ-Fe₅C₂ (h.p.) phase's lattice parameter a (11.61 ± 0.01 Å) is noticeably larger than the literature reference value by Retief (11.56 ± 0.01 Å) (Table 2).[14]

The formation of a distorted or modified χ-Fe₅C₂ phase from a Fe oxide as the carburization precursor has been previously observed in the distorted XRPD patterns and in the changes in the Hägg carbide's Curie Temperature by Cohn et al.[66] Cohn et al. suggested that some O atoms could be retained in the Hägg carbide lattice when the carburization was performed on a Fe oxide instead of a pre-reduced α-Fe.[66]

Both R-QPA and MAS quantifications are in agreement that the formed crystal lattice for the χ-Fe₅C₂ phase is dependent on whether α-Fe e.g. with catalyst treatment 340, or α-Fe₂O₃ with treatment 340 h.p. is used as the CO carburization starting material (Table 2 and Table 3). In comparison to the χ-Fe₅C₂ phase, the χ-Fe₅C₂ (h.p.) phase has i) shifted lattice parameters a, from 11.56 ± 0.01 Å to 11.61 ± 0.01 Å and c, from 5.07 ± 0.00 Å to 5.04 ± 0.00 Å as tabulated in Table 2. Furthermore, ii) the non-equivalent Fe position ratios are distorted from 1.9 : 1.8 : 1.0 to 1.3 : 1.2 : 1.0 and iii) the MAS hyperfine field corresponding to the Fe position with fraction 1.0 drops from 11.4 ± 0.3 T to 10.3 ± 0.1 T (Table 3). No precise explanations for these observations can be given at this time. That is, whether the differences in the lattices and hyperfine fields, are due to the retained O atoms in the lattice, as proposed by Cohn et al., or due to something else.[66] Additionally, a lowered lattice

ChemCatChem

Full Papers
doi.org/10.1002/cctc.202000707

**Chemistry
Europe**
European Chemical
Societies Publishing

parameter a can be observed for the χ-Fe_5C_2 phase formed from α-Fe with catalyst treatments 240–440, in comparison to Retief's lattice parameters for χ-Fe_5C_2 (Table 2). This can be tentatively explained by the used carburization conditions; i.e., with the use of pure CO carburization as opposed to Retief's H_2:CO carburization during the FTS reaction.[14]

With respect to the θ-Fe_7C_3 discrepancies, the orthorhombic crystal structure by Fruchart et al.,[100] gives a good fit for the diffraction patterns of the θ-Fe_7C_3 phase, in both peak intensity and positions. However, with different unit cell lattices than the original ones from the crystal structure's authors (Table 2). The deviations on the lattice parameters for the θ-Fe_7C_3 phase could be, in part, due to inaccurate peak position determination. The θ-Fe_7C_3 phase contents are low (Figure 5a–b), and the θ-Fe_7C_3 peaks also overlap with the more abundant χ-Fe_5C_2 (h.p.) phase (Figure 2f and Figure 3f).

Using the hexagonal crystal structure by Herbstein and Snyman,[22] instead of the orthorhombic structure by Fruchart et al.,[100] for the Fe_7C_3 phase gave a clearly worse fit to the measured XRPD patterns with R-QPA (fits are not shown). That is, the Eckström-Adcock carbide θ-Fe_7C_3 has an orthorhombic rather than a hexagonal crystal structure.[2,95] As with the θ-Fe_7C_3 phase, the diffraction peak overlap issues can also explain the large STD values for the lattice parameters of θ-Fe_3C. For the UP and Na–S 390 catalysts, the θ-Fe_3C phase diffraction peaks are poorly defined and overlap with the χ-Fe_5C_2 phase. This can be seen in Figure 2d for the phases in the UP catalysts and in Figure 3d for the phases in the Na–S catalysts. The overlap, therefore, results in large STDs in the determined lattice parameters (Table 2).

Only three of the five expected non-equivalent Fe positions could be definitely assigned for the θ-Fe_7C_3 phase on the basis of the MAS quantifications (Table 3). We assign the MAS hyperfine fields 22.4 ± 0.1 T, 19.5 ± 0.4 T and 16.3 ± 0.1 T for spectral contributions in ratios $\approx 1.0:0.9:1.8$, respectively. As based on the nominal non-equivalent Fe position ratios derived from the crystal structures, this is plausible, as the three positions can be assigned in ideal ratios of $1:1:2$ with the used orthorhombic crystal structure for the θ-Fe_7C_3 phase. For the hexagonal crystal lattice for Fe_7C_3 by Herbstein and Snyman,[22] three non-equivalent Fe positions should be assigned in a ratio $3:3:1$. This is a further indication that the hexagonal lattice is not a correct one for the Fe_7C_3 phase.[2]

The leftover two hyperfine fields, corresponding to the unassigned non-equivalent Fe positions, should then be assigned in a ratio of $2:1$ for the θ-Fe_7C_3 phase with an orthorhombic structure. However, we could not conclusively assign these two missing MAS hyperfine fields. Here, a catalyst material with a larger relative amount of the θ-Fe_7C_3 phase would be needed for properly assigning the remaining hyperfine fields for this Fe carbide phase.

Fe Carbide C Atom Order and Contents

Based on the crystal structures interpreted from literature,[2] the ε-Fe_3C phase was discussed to have C atoms occupying the Fe lattice interstitial spaces in a random, disordered manner. For the η-Fe_2C phase, the C atoms are in the interstitial spaces in a regular, ordered pattern. According to discussion by Gatte and Phillips,[101] any interstitial C atom disorder should cause spectral broadening in the measured MAS spectra. Indeed, in the fitted MAS results the expected spectral broadening can be noted from the data of Table S1 for UP and Table S2 for Na–S catalyst materials. The ε-Fe_3C phase has a mean line width of 0.75 ± 0.07 mm s^{-1} versus a mean line width of 0.49 ± 0.06 mm s^{-1} for the η-Fe_2C phase for all catalysts under study. The MAS results are thus in agreement with expectations:[2] in the ε-Fe_3C phase, C atoms occupy the interstitial spaces in a random, disordered manner,[68] while in the η-Fe_2C phase, C atoms occupy the interstitial spaces in a regular, ordered manner.[23]

The C atom content in the Fe carbide lattice can be indirectly determined from the fitted MAS hyperfine fields. Increasing amounts of C atoms in the Fe lattice interstitial spaces decrease the observed MAS hyperfine fields for each non-equivalent Fe position.[7,35,37,102,103] In Figure 8 are depicted the MAS spectral contribution weighted mean hyperfine fields for each Fe carbide phase versus the unit cell volume normalized to the Fe atoms in the phase's unit cell. By adding C atoms to the α-Fe lattice via the carburization process, the cell volume per Fe atom increases while the MAS hyperfine fields decrease (Figure 8). Furthermore, the C atom content in the Fe carbide lattices' follows decreasing MAS hyperfine fields as derived from the order of the MAS fitted, spectral contribution weighted mean hyperfine fields (Table 5 and Figure 8).

Interestingly, the distorted χ-Fe_5C_2 (h.p.) phase has the lowest averaged and weighted MAS hyperfine field, suggesting the highest C atom content in the Fe carbide lattice. Whether the observed lattice distortion effects for the χ-Fe_5C_2 (h.p.) phase with decreased MAS hyperfine fields are truly due to increased C atom content and/or, e.g. due to the retained O

Table 4. Inductively Coupled Plasma-Optical Emission Spectroscopy (ICP-OES) results of elemental analysis for ammonium Fe(III) citrate precursor $xFe(C_6H_8O_7) \cdot yNH_3$ and the calcined unpromoted (UP) and Na–S promoted (Na–S) catalyst materials.

	Elemental Analysis (weight-ppm)						
	Co	Cr	Mn	Fe	K	Na	S
$xFe(C_6H_8O_7) \cdot yNH_3$ (citrate precursor)	16	28	44	153 600	<dl	<dl	<dl
	–	–	–	162 500	57	121	9
Fe/α-Al_2O_3 (UP)	–	–	–	65 787	–	<132	<91
Fe–Na–S/α-Al_2O_3 (Na–S)	–	–	–	66 315	–	2 883	400[a]

[a] Analysis error can be >10%, <dl Below detection limit, (–) Not determined.

ChemCatChem

Full Papers
doi.org/10.1002/cctc.202000707

Chemistry Europe
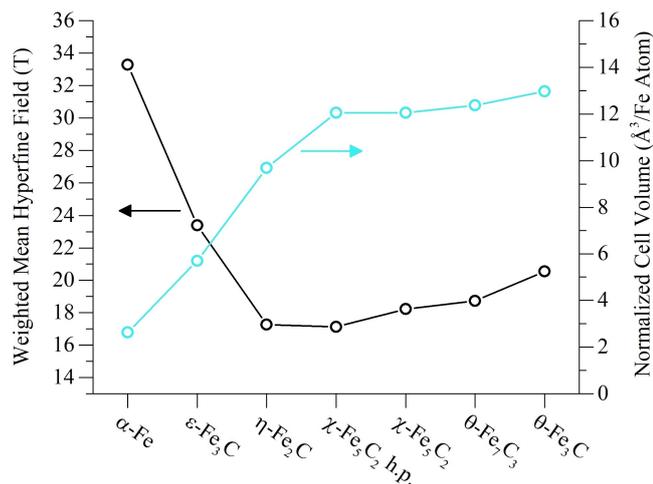European Chemical
Societies Publishing

Figure 8. Mössbauer Absorption Spectroscopy (MAS)-based spectral contribution weighted mean hyperfine fields versus Rietveld Quantitative Phase Analysis (R-QPA)-based fitted unit cell volumes normalized to Fe atoms per unit cell for each Fe carbide phase and α-Fe. Standard Deviations (STDs) for the averaged data points are smaller than the data markers, and are omitted.

Table 5. Fe carbides' relative C atom contents as derived from the order of the Mössbauer Absorption Spectroscopy (MAS) fitted, spectral contribution weighted mean hyperfine fields.

Phase	Mean hyperfine field [T]	
ε-Fe₃C	23.4 ± 0.3	"Low C"
θ-Fe₃C	20.5 ± 0.3	↓
θ-Fe₇C₃	18.7 ± 0.0	↓
χ-Fe₅C₂	18.2 ± 0.3	↓
η-Fe₂C	17.3 ± 0.3	↓
χ-Fe₅C₂ (h.p.)	17.1 ± 0.1	"High C"

atoms in the Fe carbide lattice as suggested by Cohn et al.,[66] cannot be conclusively determined based on our data.

Calculated Fe Carbide Diffraction Patterns

Examples of the Rietveld method calculated X-ray diffraction patterns of Fe carbides, used in the R-QPA fitting, are shown in Figure 9 for the UP catalyst materials. These calculated X-ray diffraction patterns hopefully serve as an aid for identifying the Fe carbide phases from XRPD patterns on past and future studies.

The R-QPA fitted, calculated X-ray diffraction patterns for the ε-Fe₃C and η-Fe₂C phases are compared in Figure 9c. The differences between the X-ray diffraction patterns for the phases are rather small. Thus, when only XRPD is used for phase identification of the ε-Fe₃C and η-Fe₂C phases, care needs to be taken for correctly identifying Fe carbides. In the inset graph of Figure 9c the weak superstructural diffraction peaks originating from the C atoms are marked with s.[68] With XRPD, the superstructural peaks are very weak, only about 1–2% of the

intensity of the most intense diffraction peak. These peaks are more pronounced with ED,[68] which is more sensitive to low atomic number elements (i.e., C atoms).

As a final remark, it is important to note that the behavior, crystal structures and X-ray diffraction patterns of the ε-Fe₃C and η-Fe₂C phases are very similar to their close, yet more stable, cousins of ε-Fe₃N and ζ-Fe₂N Fe nitrides.[104–110] A comparative study of the ε-Fe₃C and η-Fe₂C crystal structures in contrast to the structures of ε-Fe₃N and ζ-Fe₂N phases, phase properties and FTS behavior would be a good topic for future research.

Conclusions

The X-ray Powder Diffractometry (XRPD) patterns for H_2 reduced, CO carburized, supported $Fe(—Na—S)/\alpha-Al_2O_3$ catalysts were quantified with Rietveld Quantitative Phase Analysis (R-QPA) for the evaluation of the different crystalline Fe phases formed. The R-QPA results were compared to the catalysts' corresponding Mössbauer Absorption Spectroscopy (MAS) quantifications. The quantification results, obtained from both characterization techniques, were in a very good agreement. As a result, a common nomenclature between the Fe carbide crystalline structures, relative C atom contents, non-equivalent Fe position ratios and their corresponding MAS hyperfine fields could be proposed. Based on the characterization results obtained, the Fe carbides observable during the FTS reaction are listed in Table 6 with their crystal lattices.

The experimental results-based assignments of the different Fe carbides are in agreement with earlier interpretations from the literature. It is also proposed that inaccurate labelling, such as pseudo-hexagonal, "ε-carbides", (ε-)Fe₂C or ε′-Fe₂.₂C, should not be used for any Fe carbide.

Furthermore, the formation of the observed Fe carbides follows an increasing α-Fe carburization temperature. The estimated temperature regions for carbide formation from literature with comparison to the results obtained in this work are given in Table 7. The formation of the θ-Fe₇C₃ phase is not solely temperature dependent.

As explained on the basis of literature observations: a preformed (alkali-free) η-Fe₂C phase may remain stable up to 340°C, and decomposition of θ-Fe₃C into α-Fe and C atoms becomes significant at temperatures > 527°C in the absence of

Table 6. Fe carbides with their crystal lattices that are observable in Fischer-Tropsch Synthesis reaction.

Phase	Crystal System	Space Group
ε-Fe₃C,	Hexagonal,	*P6₃22* (182)
η-Fe₂C,	Orthorhombic,	*Pnnm* (58)
χ-Fe₅C₂,	Monoclinic,	*C2/c* (15)
θ-Fe₃C,	Orthorhombic,	*Pnma* (62)
θ-Fe₇C₃,	Orthorhombic,	*Pnma* (62)

Table 7. Fe carbide formation temperature ranges from α-Fe.

ε-Fe₃C	<	η-Fe₂C	<	χ-Fe₅C₂	<	θ-Fe₃C
100–265°C		160–300°C		240–420°C		350–500°C

ChemCatChem

Full Papers
doi.org/10.1002/cctc.202000707

Chemistry Europe
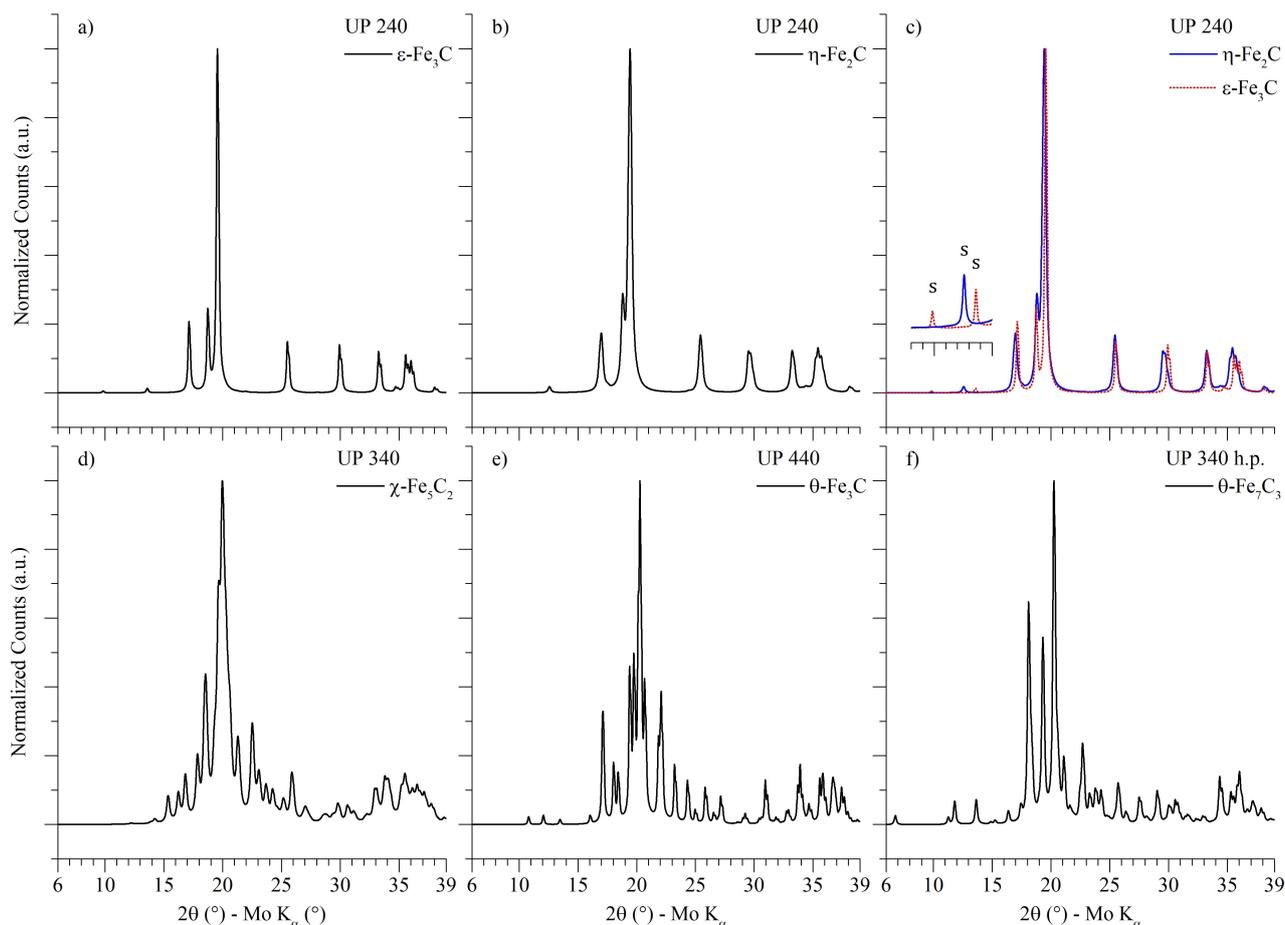European Chemical
Societies Publishing

Figure 9. Rietveld method calculated X-ray diffraction patterns of Fe carbide phases compared for UP (Fe/α-Al$_2$O$_3$) catalyst materials. The Fe carbides as after catalyst treatment a) ε-Fe$_3$C 240, b) η-Fe$_2$C 240, c) ε-Fe$_3$C and η-Fe$_2$C 240, d) χ-Fe$_5$C$_2$ 340, e) θ-Fe$_3$C 440 and f) θ-Fe$_7$C$_3$ 340 h.p. Pattern normalization was done to the most intense diffraction peak.

a carbide oxidation shell. The presence of a shell can increase the thermal stability of the θ-Fe$_3$C phase up to 600 °C.

It is speculated that the formation of the θ-Fe$_7$C$_3$ phase is related to the presence of CO$_2$. The θ-Fe$_7$C$_3$ phase could only be formed with a high-pressure carburization (i.e., 340 °C, 25 bar, CO) with Fe oxide (α-Fe$_2$O$_3$/α-Al$_2$O$_3$) as the carburization starting material. Additionally, a distinctly distorted χ-Fe$_5$C$_2$ (h.p.) Hägg carbide phase could be observed with both R-QPA and MAS after the high-pressure treatment, in addition to the presence of the θ-Fe$_7$C$_3$ phase. The formation temperature of 340 °C for the θ-Fe$_7$C$_3$ phase matches literature observations.

With CO carburization of α-Fe, the added Na—S promotion did not affect the lattice parameters, the MAS hyperfine fields or the formed phase quantities of any of the Fe carbides. In addition, the Fe carbide crystallite diameters remained largely unaffected by the Na—S promotion. In literature, added alkali is occasionally cited to improve the Fe carbide formation; however, our results do not support this view. The literature observations were explained to be due to an enhanced reduction of Fe oxides with CO when alkali is present. That is, alkali improves *the Fe oxide reduction step with CO not the Fe carburization step*. As the carburization treatments were

performed with α-Fe as the starting material - with the exception of the high-pressure treatment – the lack of observable Na—S promotion effect on the Fe carburization can be accounted for.

As primary effects on Fe carburization, the added Na—S promotion i) increased the Fe oxidation tendency, presumably by O from the CO dissociation acting as oxidation agent, with short, low temperature CO carburization treatments ($\leq$290 °C, $\leq$3 h) and ii) increased the formation of the χ-Fe$_5$C$_2$ phase relative to the θ-Fe$_3$C phase at temperatures >390 °C.

Experimental Section

Catalyst Preparation

Catalyst Synthesis

Supported catalyst materials with a nominal 7 weight percent (wt-%) Fe loading, with and without Na—S promotion, were prepared via Incipient Wetness Impregnation (IWI) of an alpha-alumina (α-Al$_2$O$_3$) support (BASF, 7 m^2/g, 212–425 µm particle size). Ammonium Fe(III) citrate (Acros, 211840010) was used as the Fe precursor, Fe(II)

These are not the final page numbers! ↗↗

ChemCatChem

Full Papers
doi.org/10.1002/cctc.202000707

**Chemistry
Europe**
European Chemical
Societies Publishing

sulfate heptahydrate (Sigma-Aldrich, 215422) as the S precursor and Na tribasic citrate dihydrate (Sigma-Aldrich, S4641) as the Na precursor. The elemental analysis of the ammonium Fe(III) citrate Fe precursor was performed using Inductively Coupled Plasma Optical Emission Spectroscopy (ICP-OES). The ICP-OES results are summarized in Table 4.

Catalyst Calcination

Calcination of the catalysts was done under flowing air in an open quartz vessel by heating ($10\,°C/min$) the material from room temperature to $500\,°C$, and holding the temperature for 6 h. In order to avoid gas diffusion limitations, the catalyst materials were calcined in batches of ~ 2.8 g. Each batch lost $\sim 21\%$ of its weight during the calcination step. The calcined catalyst materials were combined for each of the unpromoted and Na–S promoted catalyst batches and re-sieved to the catalyst particle fraction of 212–425 µm in order to obtain the ready, calcined catalyst materials. The results for the elemental contents of Fe, Na and S using ICP-OES analysis on the two sets of the calcined catalyst materials are included in Table 4.

Catalyst Reduction and Carburization

Catalyst Reduction

The calcined catalyst materials were reduced into metallic, zerovalent α-Fe on the $\alpha-Al_2O_3$ support prior to carburization with CO. For each reduction or carburization treatment, ~ 600 mg of calcined, unpromoted or Na–S promoted catalyst material was loaded into a plug flow quartz reactor. The reactor was heated up ($10\,°C/min$) from room temperature to $400\,°C$ under $N_2:H_2$ flow (20 ml/min $N_2 + 12$ ml/min H_2, at atmospheric pressure) and held at $400\,°C$ for 5 h. After the 5 h reduction step, the reactor was cooled down to $200\,°C$ under the set $N_2:H_2$ flow and let to stabilize for 15 min. For the catalysts only reduced with H_2, without any subsequent CO carburization step, the reactor was cooled down to room temperature under the $N_2:H_2$ flow and flushed with N_2 for several hours to passivate the catalyst.

Catalyst Carburization at 1 bar

The H_2 reduced catalyst materials, either with or without Na–S promotion, were subsequently carburized with CO without removing the catalyst from the reactor after the H_2 reduction step. Under the set $N_2:H_2$ flow, the reduced catalyst was heated up ($10\,°C/min$) from $200\,°C$ to a desired carburization temperature. Upon reaching the desired carburization temperature, the $N_2:H_2$ flow was switched to pure CO flow (20 ml/min, at atmospheric pressure). The carburization temperatures and times used were: $240\,°C$ (2 h), $290\,°C$ (3 h), $340\,°C$ (16 h), $390\,°C$ (16 h) and $440\,°C$ (16 h). After the desired carburization period, the CO flow was switched to pure N_2 and the reactor was cooled down to room temperature and flushed with N_2 for several hours.

Catalyst Carburization at 25 bar

Calcined, unpromoted and Na–S promoted catalyst materials were *carburized directly without the H_2 reduction step* at an elevated pressure. Around 600 mg of calcined, unpromoted or Na–S promoted, catalyst material was loaded into a plug flow quartz reactor. Under a flow of He (5 ml/min), the reactor was heated to ($10\,°C/min$) $120\,°C$ from the room temperature. The reactor was pressurized at $120\,°C$ to 25 bar total pressure with CO:He flow

(40 ml/min CO + 5 ml/min He) over a period of 2 h. The reactor was then heated up ($10\,°C/min$) to $340\,°C$. The unpromoted catalyst material was carburized for 120 h and the Na–S promoted catalyst for 168 h at $340\,°C$ at the 25 bar total CO:He pressure. After the carburization period, the reactor was first cooled down to room temperature after which the gas flow was switched to Ar (12 ml/min) and the pressure reduced from 25 bar to atmospheric pressure. All of the gases used in this study (Ar, He, N_2, H_2) were grade 5.0 purity (99.999% pure), with the exception of the CO gas which had the purity grade of 2.5 (99.5% pure). All of the used gases were supplied by Linde Gas Benelux.

Catalyst Characterization

Mössbauer Absorption Spectroscopy

Ex-situ transmission ^{57}Fe MAS was performed at room temperature (300 K) with a conventional constant-acceleration spectrometer using a ^{57}Co (Rh) source. Velocity calibration was carried out using an α-Fe foil. The MAS spectra were fitted using the Mosswinn 4.0 software.[111] Non-equivalent Fe position ratios were determined from the fitted relation of spectral contributions for each of the Fe carbide phases' hyperfine fields.

X-ray Powder Diffractometry

The XRPD patterns for the prepared catalyst materials were measured ex-situ using a Bruker D8 Discover instrument in Debye-Scherrer transmission (capillary) geometry with a Mo ($K_{\alpha 1}$ 0.709 Å) source. The use of high energy Mo radiation in capillary geometry is especially suitable for phase quantification purposes.[52] A Göbel-mirror was used to focus a near-parallel $\approx 600 \times 15\,000$ µm (height × width) X-ray beam on a static i.e. non-rotating 1000 µm (outer diameter, wall thickness 10 µm) borosilicate capillary loaded with the catalyst material. An energy dispersive LynxEye XE Position Sensitive Detector (PSD) was used, only accepting the diffracted X-ray photons originating from the Mo K_α emission lines. 2.5° Soller slits were used on source and detector sides.

2θ range of 6–39° with step size 0.015° and exposure time of 30 s per step, were used for each sample measurement. Prior to each measurement, the sample capillary was manually rotated and shortly test measured in order to verify the powder diffraction conditions. No changes in diffraction intensities were observed following the capillary rotation, thus, all of the measured samples contained a sufficient amount of diffracting Fe crystallites for proper powder diffraction measurements. The term X-ray Powder Diffractometry (XRPD) is used to refer to X-ray diffraction phenomena based characterization experiments that are done under powder diffraction conditions.[112]

For each measurement, the sample capillary was focused to the incident X-ray beam for maximum diffraction intensity. Air scattering contribution to the low angle background in the diffraction pattern was reduced by installing a stainless steel plate on top of the sample capillary during the measurements.

The details of the applied R-QPA method for quantifying the phases from the measured powder diffraction patterns are given in the Supporting information.

Acknowledgements

Conflict of Interest

The authors declare no conflict of interest.

[1] J. W. Niemantsverdriet, A. M. van der Kraan, *J. Catal.* **1981**, *72*, 385–388.
[2] P. P. Paalanen, B. M. Weckhuysen, *ChemCatChem* **2020**, *12*, 4202–4223.
[3] E. de Smit, B. M. Weckhuysen, *Chem. Soc. Rev.* **2008**, *37*, 2758–2781.
[4] J. W. Niemantsverdriet, A. M. van der Kraan, W. L. van Dijk, H. S. van der Baan, *J. Phys. Chem.* **1980**, *84*, 3363–3370.
[5] E. de Smit, F. Cinquini, A. M. Beale, O. V. Safonova, W. van Beek, P. Sautet, B. M. Weckhuysen, *J. Am. Chem. Soc.* **2010**, *132*, 14928–14941.
[6] R. M. Stanfield, W. N. Delgass, *J. Catal.* **1981**, *72*, 37–50.
[7] G. Le Caër, J. M. Dubois, M. Pijolat, V. Perrichon, P. Bussière, *J. Phys. Chem.* **1982**, *86*, 4799–4808.
[8] H. Jung, W. J. Thomson, *J. Catal.* **1992**, *134*, 654–667.
[9] X.-W. Liu, Z. Cao, S. Zhao, R. Gao, Y. Meng, J.-X. Zhu, C. Rogers, C.-F. Huo, Y. Yang, Y.-W. Li, et al., *J. Phys. Chem. C* **2017**, *121*, 21390–21396.
[10] L. J. E. Hofer, E. M. Cohn, W. C. Peebles, *J. Am. Chem. Soc.* **1949**, *71*, 189–195.
[11] G. H. Barton, B. Gale, *Acta Crystallogr.* **1964**, *17*, 1460–1462.
[12] Z. Yang, M. Luo, Q. Liu, B. Shi, *Catal. Lett.* **2020**, DOI 10.1007/s10562-020-03147-6.
[13] M. J. Duggin, L. J. E. Hofer, *Nature* **1966**, *212*, 248–248.
[14] J. J. Retief, *Powder Diffr.* **1999**, *14*, 130–132.
[15] P. Wang, W. Chen, F. Chiang, A. I. Dugulan, Y. Song, R. Pestman, K. Zhang, J. Yao, B. Feng, P. Miao, et al., *Sci. Adv.* **2018**, *4*, eaau2947.
[16] T. A. Wezendonk, X. Sun, A. I. Dugulan, A. J. F. van Hoof, E. J. M. Hensen, F. Kapteijn, J. Gascon, *J. Catal.* **2018**, *362*, 106–117.
[17] S. Pérez, F. Mondragón, A. Moreno, *Appl. Catal. A* **2019**, *587*, 117264.
[18] L. J. E. Hofer, E. M. Cohn, *Nature* **1951**, *167*, 977–978.
[19] L. J. E. Hofer, *Nature of the Carbides of Iron*, Washington D. C. **1966**.
[20] M. E. Dry, *Catal. - Sci. Technol.* (Eds.: J. R. Anderson, M. Boudart), Springer-Verlag, Berlin **1981**, pp. 159–256.
[21] H. C. Eckstrom, W. A. Adcock, *J. Am. Chem. Soc.* **1950**, *72*, 1042–1043.
[22] F. H. Herbstein, J. A. Snyman, *Inorg. Chem.* **1964**, *3*, 894–896.
[23] Y. Hirotsu, S. Nagakura, *Acta Metall.* **1972**, *20*, 645–655.
[24] Y. Hirotsu, S. Nagakura, *Trans. Jpn. Inst. Met.* **1974**, *15*, 129–134.
[25] E. de Smit, A. M. Beale, S. Nikitenko, B. M. Weckhuysen, *J. Catal.* **2009**, *262*, 244–256.
[26] J. F. Shultz, W. K. Hall, B. Seligman, R. B. Anderson, *J. Am. Chem. Soc.* **1955**, *77*, 213–221.
[27] J. F. Shultz, W. K. Hall, T. A. Dubs, R. B. Anderson, *J. Am. Chem. Soc.* **1956**, *78*, 282–285.
[28] S. Tajima, S. Hirano, *Jpn. J. Appl. Phys.* **1990**, *29*, 662–668.
[29] R. Dictor, A. T. Bell, *J. Catal.* **1986**, *97*, 121–136.
[30] R. J. O'Brien, L. Xu, D. R. Milburn, Y.-X. Li, K. J. Klabunde, B. H. Davis, *Top. Catal.* **1995**, *2*, 1–15.
[31] W. Ning, N. Koizumi, H. Chang, T. Mochizuki, T. Itoh, M. Yamada, *Appl. Catal. A* **2006**, *312*, 35–44.
[32] R. P. Mogorosi, N. Fischer, M. Claeys, E. van Steen, *J. Catal.* **2012**, *289*, 140–150.
[33] A. Königer, C. Hammerl, M. Zeitler, B. Rauschenbach, *Phys. Rev. B* **1997**, *55*, 8143–8147.
[34] E. Boellaard, A. M. van der Kraan, J. W. Geus, *Appl. Catal. A* **1996**, *147*, 229–245.
[35] M. Pijolat, V. Perrichon, P. Bussière, *J. Catal.* **1987**, *107*, 82–91.
[36] J. A. Amelse, J. B. Butt, L. H. Schwartz, *J. Phys. Chem.* **1978**, *82*, 558–563.
[37] X.-W. Liu, S. Zhao, Y. Meng, Q. Peng, A. K. Dearden, C.-F. Huo, Y. Yang, Y.-W. Li, X.-D. Wen, *Sci. Rep.* **2016**, *6*, 26184.
[38] D. L. Williamson, K. Nakazawa, G. Krauss, *Metall. Trans. A* **1979**, *10*, 1351–1363.
[39] G. F. Botes, T. C. Bromfield, R. L. J. Coetzer, R. Crous, P. Gibson, A. C. Ferreira, *Catal. Today* **2016**, *275*, 40–48.
[40] R. Crous, T. C. Bromfield, S. Booyens (Sasol Technology), WO2010066386, **2010**.
[41] J. Y. Johnson, GB322284, **1929**.
[42] H. M. Torres Galvis, J. H. Bitter, C. B. Khare, M. Ruitenbeek, A. I. Dugulan, K. P. de Jong, *Science* **2012**, *335*, 835–838.
[43] V. R. R. Pendyala, U. M. Graham, G. Jacobs, H. H. Hamdeh, B. H. Davis, *Catal. Lett.* **2014**, *144*, 1704–1716.
[44] X. An, B. Wu, H.-J. Wan, T.-Z. Li, Z.-C. Tao, H.-W. Xiang, Y.-W. Li, *Catal. Commun.* **2007**, *8*, 1957–1962.
[45] B. H. Toby, *Powder Diffr.* **2006**, *21*, 67–70.
[46] S. Janbroers, J. N. Louwen, H. W. Zandbergen, P. J. Kooyman, *J. Catal.* **2009**, *268*, 235–242.
[47] M. D. Shroff, A. K. Datye, *Catal. Lett.* **1996**, *37*, 101–106.
[48] J. Xie, H. M. Torres Galvis, A. C. J. Koeken, A. Kirilin, A. I. Dugulan, M. Ruitenbeek, K. P. de Jong, *ACS Catal.* **2016**, *6*, 4017–4024.
[49] J. Li, X. Cheng, C. Zhang, Q. Chang, J. Wang, X. Wang, Z. Lv, W. Dong, Y. Yang, Y. Li, *Appl. Catal. A* **2016**, *528*, 131–141.
[50] J. A. Amelse, G. Grynkewich, J. B. Butt, L. H. Schwartz, *J. Phys. Chem.* **1981**, *85*, 2484–2488.
[51] N. Sirimanothan, H. H. Hamdeh, Y. Zhang, B. H. Davis, *Catal. Lett.* **2002**, *82*, 181–191.
[52] L. León-Reina, M. García-Maté, G. Álvarez-Pinazo, I. Santacruz, O. Vallcorba, A. G. De la Torre, M. A. G. Aranda, *J. Appl. Crystallogr.* **2016**, *49*, 722–735.
[53] L. León-Reina, A. G. De la Torre, J. M. Porras-Vázquez, M. Cruz, L. M. Ordonez, X. Alcobé, F. Gispert-Guirado, A. Larrañaga-Varga, M. Paul, T. Fuellmann, et al., *J. Appl. Crystallogr.* **2009**, *42*, 906–916.
[54] F. M. Michel, L. Ehm, S. M. Antao, P. L. Lee, P. J. Chupas, G. Liu, D. R. Strongin, M. A. A. Schoonen, B. L. Phillips, J. B. Parise, *Science* **2007**, *316*, 1726–1729.
[55] W. K. Jozwiak, E. Kaczmarek, T. P. Maniecki, W. Ignaczak, W. Maniukiewicz, *Appl. Catal. A* **2007**, *326*, 17–27.
[56] H. H. Podgurski, J. T. Kummer, T. W. DeWitt, P. H. Emmett, *J. Am. Chem. Soc.* **1950**, *72*, 5382–5388.
[57] S. Krishnamoorthy, A. Li, E. Iglesia, *Catal. Lett.* **2002**, *80*, 77–86.
[58] B. H. Davis, *Catal. Today* **2009**, *141*, 25–33.
[59] J. F. Shultz, M. Abelson, K. C. Stein, R. B. Anderson, *J. Phys. Chem.* **1959**, *63*, 496–500.
[60] R. J. O'Brien, L. Xu, R. L. Spicer, B. H. Davis, *Energy Fuels* **1996**, *10*, 921–926.
[61] D. B. Bukur, K. Okabe, M. P. Rosynek, C. P. Li, D. J. Wang, K. R. P. M. Rao, G. P. Huffman, *J. Catal.* **1995**, *155*, 353–365.
[62] H. Arakawa, A. T. Bell, *Ind. Eng. Chem. Process Des. Dev.* **1983**, *22*, 97–103.
[63] R. G. Olsson, E. T. Turkdogan, *Metall. Trans.* **1974**, *5*, 21–26.
[64] M. E. Dry, T. Shingles, C. S. van H Botha, *J. Catal.* **1970**, *17*, 341–346.
[65] M. E. Dry, T. Shingles, L. J. Boshoff, C. S. van H Botha, *J. Catal.* **1970**, *17*, 347–354.
[66] E. M. Cohn, E. H. Bean, M. Mentser, L. J. E. Hofer, A. Pontello, W. C. Peebles, K. H. Jack, *J. Appl. Chem.* **1955**, *5*, 418–425.
[67] T. F. Berry, R. N. Ames, R. B. Snow, *J. Am. Ceram. Soc.* **1956**, *39*, 308–318.
[68] S. Nagakura, *J. Phys. Soc. Jpn.* **1959**, *14*, 186–195.
[69] G. B. Raupp, W. N. Delgass, *J. Catal.* **1979**, *58*, 348–360.
[70] L. M. Tau, S. Borcar, D. Bianchi, C. O. Bennett, *J. Catal.* **1984**, *87*, 36–54.

[71] K. Xu, B. Sun, J. Lin, W. Wen, Y. Pei, S. Yan, M. Qiao, X. Zhang, B. Zong, *Nat. Commun.* **2014**, *5*, 5783.

[72] F. Jiang, M. Zhang, B. Liu, Y. Xu, X. Liu, *Catal. Sci. Technol.* **2017**, *7*, 1245–1265.

[73] T. Riedel, H. Schulz, G. Schaub, K.-W. Jun, J.-S. Hwang, K.-W. Lee, *Top. Catal.* **2003**, *26*, 41–54.

[74] S. Nagakura, Y. Hirotsu, M. Kusunoki, T. Suzuki, Y. Nakamura, *Metall. Trans. A* **1983**, *14*, 1025–1031.

[75] E. Bauer-Grosse, G. Le Caër, *J. Phys. F* **1986**, *16*, 399–406.

[76] S. Nagakura, T. Suzuki, M. Kusunoki, *Trans. Jpn. Inst. Met.* **1981**, *22*, 699–709.

[77] H. E. du Plessis, J. P. R. de Villiers, G. J. Kruger, A. Steuwer, M. Brunelli, *J. Synchrotron Radiat.* **2011**, *18*, 266–271.

[78] E. M. Cohn, L. J. E. Hofer, *J. Am. Chem. Soc.* **1950**, *72*, 4662–4664.

[79] I. G. Wood, L. Vočadlo, K. S. Knight, D. P. Dobson, W. G. Marshall, G. D. Price, J. Brodholt, *J. Appl. Crystallogr.* **2004**, *37*, 82–90.

[80] E. de Smit, M. M. van Schooneveld, F. Cinquini, H. Bluhm, P. Sautet, F. M. F. de Groot, B. M. Weckhuysen, *Angew. Chem. Int. Ed.* **2011**, *50*, 1584–1588; *Angew. Chem.* **2011**, *123*, 1622–1626.

[81] A. Bordet, A. Soulantika, B. Chaudret (Institut National des Sciences Appliquees de Toulouse), WO 2017/103492, **2017**.

[82] J. Li, X. Cheng, C. Zhang, Y. Yang, Y. Li, *J. Mol. Catal. A* **2015**, *396*, 174–180.

[83] F. J. Berry, M. R. Smith, *J. Chem. Soc. Faraday Trans. 1* **1989**, *85*, 467–477.

[84] M. C. Ribeiro, G. Jacobs, B. H. Davis, D. C. Cronauer, A. J. Kropf, C. L. Marshall, *J. Phys. Chem. C* **2010**, *114*, 7895–7903.

[85] W. Ngantsoue-Hoc, Y. Zhang, R. J. O'Brien, M. Luo, B. H. Davis, *Appl. Catal. A* **2002**, *236*, 77–89.

[86] C. Ratnasamy, J. P. Wagner, *Catal. Rev.* **2009**, *51*, 325–440.

[87] B. W. Krupay, Y. Amenomiya, *J. Catal.* **1981**, *67*, 362–370.

[88] Y. Amenomiya, G. Pleizier, *J. Catal.* **1982**, *76*, 345–353.

[89] R. B. Anderson, F. S. Karn, J. F. Shultz, *J. Catal.* **1965**, *4*, 56–63.

[90] E. K. Towett, K. D. Shepherd, G. Cadisch, *Sci. Total Environ.* **2013**, *463–464*, 374–388.

[91] A. Tsuzuki, S. Sago, S.-I. Hirano, S. Naka, *J. Mater. Sci.* **1984**, *19*, 2513–2518.

[92] X.-X. Bi, B. Ganguly, G. P. Huffman, F. E. Huggins, M. Endo, P. C. Eklund, *J. Mater. Res.* **1993**, *8*, 1666–1674.

[93] Y. Yamada, H. Yoshida, K. Kouno, Y. Kobayashi, *J. Phys. Conf. Ser.* **2010**, *217*, 012096.

[94] A. R. Sethuraman, *Nanostruct. Mater.* **1994**, *4*, 79–92.

[95] M. Audier, P. Bowen, W. Jones, *J. Cryst. Growth* **1983**, *63*, 125–134.

[96] W. J. Lywood, M. V. Twigg (ICI PLC), EP0361648, **1990**.

[97] M. Luo, B. H. Davis, *Appl. Catal. A* **2003**, *246*, 171–181.

[98] C. Rhodes, G. J. Hutchings, A. M. Ward, *Catal. Today* **1995**, *23*, 43–58.

[99] R. B. Anderson, L. J. E. Hofer, E. M. Cohn, B. Seligman, *J. Am. Chem. Soc.* **1951**, *73*, 944–946.

[100] R. Fruchart, J. P. Senateur, J. P. Bouchaud, A. Michel, *Bull. Soc. Chim. Fr.* **1965**, *2*, 392.

[101] R. R. Gatte, J. Phillips, *J. Catal.* **1987**, *104*, 365–374.

[102] J. Foct, J. P. Senateur, J. M. Dubois, G. Le Caër, *J. Phys. Colloq.* **1979**, *40*, 647–649.

[103] J. M. Dubois, G. Le Caër, *Acta Metall.* **1977**, *25*, 609–618.

[104] J. F. Shultz, M. Abelson, L. Shaw, R. B. Anderson, *Ind. Eng. Chem.* **1957**, *49*, 2055–2060.

[105] R. Niewa, D. Rau, A. Wosylus, K. Meier, M. Hanfland, M. Wessel, R. Dronskowski, D. A. Dzivenko, R. Riedel, U. Schwarz, *Chem. Mater.* **2009**, *21*, 392–398.

[106] A. Leineweber, S. Shang, Z.-K. Liu, M. Widenmeyer, R. Niewa, *Z. Kristallogr.* **2012**, *227*, 207–220.

[107] K. H. Jack, *Acta Crystallogr.* **1952**, *5*, 404–411.

[108] D. Rechenbach, H. Jacobs, *J. Alloys Compd.* **1996**, *235*, 15–22.

[109] H. Jacobs, D. Rechenbach, U. Zachwieja, *J. Alloys Compd.* **1995**, *227*, 10–17.

[110] S. Nagakura, K. Tanehashi, *J. Phys. Soc. Jpn.* **1968**, *25*, 840–846.

[111] Z. Klencsár, E. Kuzmann, A. Vértes, *J. Radioanal. Nucl. Chem.* **1996**, *210*, 105–118.

[112] R. Jenkins, R. L. Snyder, *Introduction to X-Ray Powder Diffractometry*, John Wiley & Sons, Inc., Hoboken, NJ, USA **1996**.

[113] K. Momma, F. Izumi, *J. Appl. Crystallogr.* **2011**, *44*, 1272–1276.

FULL PAPERS

*P. P. Paalanen, S. H. van Vreeswijk, Dr. A. I. Dugulan, Prof. Dr. B. M. Weckhuysen**

Identification of Iron Carbides in Fe(−Na−S)/α-Al₂O₃ Fischer-Tropsch Synthesis Catalysts with X-ray Powder Diffractometry and Mössbauer Absorption Spectroscopy
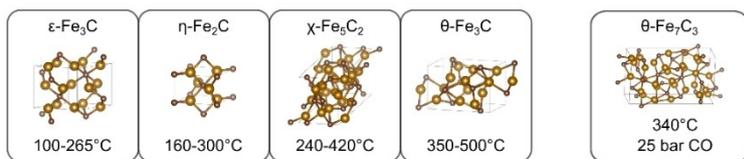
Identification of catalyst using spectroscopy: Fischer-Tropsch Synthesis (FTS) reaction with Fe-based catalysts is a versatile method for converting a $CO + H_2$ gas mixture into hydrocarbons. Fe carbides, the FTS active Fe phases, are identified and their properties assigned using both X-ray Powder Diffractometry (XRPD) with Rietveld Quantitative Phase Analysis (R-QPA) and Mössbauer Absorption Spectroscopy (MAS). Effect of Na−S promotion on the Fe carbide formation is further investigated.